IEC TR 63401-2

Edition 1.0 2022-06

TECHNICAL REPORT

colour inside

Dynamic characteristics of inverter-based resources in bulk power systems – Part 2: Sub- and super-synchronous control interactions

IEC TR 63401-2:2022-06(en)

IEC Secretariat
3, rue de Varembé
CH-1211 Geneva 20
Switzerland

Tel.: +41 22 919 02 11
info@iec.ch
www.iec.ch

About the IEC
The International Electrotechnical Commission (IEC) is the leading global organization that prepares and publishes International Standards for all electrical, electronic and related technologies.

About IEC publications
The technical content of IEC publications is kept under constant review by the IEC. Please make sure that you have the latest edition, a corrigendum or an amendment might have been published.

IEC publications search - webstore.iec.ch/advsearchform
The advanced search enables to find IEC publications by a variety of criteria (reference number, text, technical committee, …). It also gives information on projects, replaced and withdrawn publications.

IEC Just Published - webstore.iec.ch/justpublished
Stay up to date on all new IEC publications. Just Published details all new publications released. Available online and once a month by email.

IEC Customer Service Centre - webstore.iec.ch/csc
If you wish to give us your feedback on this publication or need further assistance, please contact the Customer Service Centre: sales@iec.ch.

IEC Products & Services Portal - products.iec.ch
Discover our powerful search engine and read freely all the publications previews. With a subscription you will always have access to up to date content tailored to your needs.

Electropedia - www.electropedia.org
The world's leading online dictionary on electrotechnology, containing more than 22 300 terminological entries in English and French, with equivalent terms in 19 additional languages. Also known as the International Electrotechnical Vocabulary (IEV) online.

IEC TR 63401-2

Edition 1.0 2022-06

TECHNICAL REPORT

colour inside

Dynamic characteristics of inverter-based resources in bulk power systems – Part 2: Sub- and super-synchronous control interactions

INTERNATIONAL
ELECTROTECHNICAL
COMMISSION

ICS 27.160, 27.180, 29.020

ISBN 978-2-8322-3929-2

Warning! Make sure that you obtained this publication from an authorized distributor.

CONTENTS

INTERNATIONAL ELECTROTECHNICAL COMMISSION

_____

DYNAMIC CHARACTERISTICS OF INVERTER-BASED RESOURCES IN BULK POWER SYSTEMS –

Part 2: Sub- and super-synchronous control interactions

FOREWORD

1) The International Electrotechnical Commission (IEC) is a worldwide organization for standardization comprising all national electrotechnical committees (IEC National Committees). The object of IEC is to promote international co-operation on all questions concerning standardization in the electrical and electronic fields. To this end and in addition to other activities, IEC publishes International Standards, Technical Specifications, Technical Reports, Publicly Available Specifications (PAS) and Guides (hereafter referred to as "IEC Publication(s)"). Their preparation is entrusted to technical committees; any IEC National Committee interested in the subject dealt with may participate in this preparatory work. International, governmental and non-governmental organizations liaising with the IEC also participate in this preparation. IEC collaborates closely with the International Organization for Standardization (ISO) in accordance with conditions determined by agreement between the two organizations.
2) The formal decisions or agreements of IEC on technical matters express, as nearly as possible, an international consensus of opinion on the relevant subjects since each technical committee has representation from all interested IEC National Committees.
3) IEC Publications have the form of recommendations for international use and are accepted by IEC National Committees in that sense. While all reasonable efforts are made to ensure that the technical content of IEC Publications is accurate, IEC cannot be held responsible for the way in which they are used or for any misinterpretation by any end user.
4) In order to promote international uniformity, IEC National Committees undertake to apply IEC Publications transparently to the maximum extent possible in their national and regional publications. Any divergence between any IEC Publication and the corresponding national or regional publication shall be clearly indicated in the latter.
5) IEC itself does not provide any attestation of conformity. Independent certification bodies provide conformity assessment services and, in some areas, access to IEC marks of conformity. IEC is not responsible for any services carried out by independent certification bodies.
6) All users should ensure that they have the latest edition of this publication.
7) No liability shall attach to IEC or its directors, employees, servants or agents including individual experts and members of its technical committees and IEC National Committees for any personal injury, property damage or other damage of any nature whatsoever, whether direct or indirect, or for costs (including legal fees) and expenses arising out of the publication, use of, or reliance upon, this IEC Publication or any other IEC Publications.
8) Attention is drawn to the Normative references cited in this publication. Use of the referenced publications is indispensable for the correct application of this publication.
9) Attention is drawn to the possibility that some of the elements of this IEC Publication may be the subject of patent rights. IEC shall not be held responsible for identifying any or all such patent rights.

IEC TR 63401-2 has been prepared by subcommittee SC 8A: Grid Integration of renewable energy generation, of IEC technical committee TC 8: Systems aspects of electrical energy supply. It is a Technical Report.

The text of this Technical Report is based on the following documents:

Draft TR	Report on voting
8A/99/DTR	8A/103/RVDTR

Full information on the voting for its approval can be found in the report on voting indicated in the above table.

The language used for the development of this Technical Report is English.

This document was drafted in accordance with ISO/IEC Directives, Part 2, and developed in accordance with ISO/IEC Directives, Part 1 and ISO/IEC Directives, IEC Supplement, available at www.iec.ch/members_experts/refdocs. The main document types developed by IEC are described in greater detail at www.iec.ch/standardsdev/publications.

A list of all parts in the IEC 63401 series, published under the general title *Dynamic characteristics of inverter-based resources in bulk power systems*, can be found on the IEC website.

The committee has decided that the contents of this document will remain unchanged until the stability date indicated on the IEC website under webstore.iec.ch in the data related to the specific document. At this date, the document will be

- reconfirmed,
- withdrawn,
- replaced by a revised edition, or
- amended.

IMPORTANT – The "colour inside" logo on the cover page of this document indicates that it contains colours which are considered to be useful for the correct understanding of its contents. Users should therefore print this document using a colour printer.

INTRODUCTION

Advancements in power electronic converters have led to an increased proportion of converter based renewable power generators in modern electric power systems. Power electronic converters use multi-time scale converter control structures to achieve smooth grid connection. Such control interactions cause oscillation with the frequency ranging from a few hertz to several kilohertz, which can interact with other converter-based devices or system components such as static compensators (STATCOM), series capacitors and weak AC grids. The interactions of converter control with series-compensated or weak AC grid cause oscillation in the subsynchronous and its complementary supper synchronous frequency ranges, named as sub- and super-synchronous control interaction or simply sub-synchronous control interaction (SSCI).

In the past decade, several incidents have been reported where wind turbine and photovoltaic (PV) converter controls interacted with series-compensated or weak AC grids at subsynchronous and/or supersynchronous frequencies. Post-event investigations have shown that the converter controls actively participate in these interactions. Unlike classical sub-synchronous resonance (SSR), SSCI is a system-wide phenomenon rather than a localized converter control issue. The mechanism and characteristics of SSCI are greatly influenced by converter control structures and parameters, generation resource intermittency, network topology change, grid strength, etc. Such factors distinguish the converter control participated interactions in converter-based generators from the classic SSR phenomenon associated with the conventional power generators. The oscillation caused by SSCI seriously threatens the stable and reliable operation of wind power systems.

Power systems with high-penetration of power electronic converters face a variety of oscillatory stability issues. Power electronic converter-based components such as converter-based wind turbine generators (WTGs), photovoltaic (PV), flexible AC transmission system (FACTS) and high voltage DC (HVDC) can interact with each other and/or with the series-compensated or weak AC networks. As a result of such interactions, oscillation from a few hertz to tens or hundreds of hertz could be triggered, as illustrated in Figure 1.

The interaction between doubly-fed induction generators (DFIGs) and series compensated transmission lines was first reported in the electric reliability council of Texas (ERCOT) wind power system in 2009. The frequency of triggered oscillation was 20 Hz to 30 Hz. Later on, from 2010 to 2016, frequent oscillation events were reported between DFIG and series-compensated network in the Guyuan system located in Hebei, China. In 2015, a new type of interaction was reported in the Hami wind power system in Western China. Post-event investigations showed that the full-scale converter (FSC) interacted with the weak AC grid causing strong sub- and super-synchronous oscillation. The frequency of oscillation originating from the FSC wind turbines matched with the shafts' natural frequencies of the nearby steam turbine generators, which resulted in intense torsional vibrations. In 2019, a power outage event in the UK's National Grid was also found to have been worsened by a 9 Hz oscillation. The converter controls of the FSCs in the Hornsea offshore wind farm participated in the event and amplified the negative resistance effect, which led to the sudden shutdown of the wind farm.

The frequency of oscillation triggered by the interactions between converter generators (e.g. wind or PV) and series-compensated or weak AC grid falls in the range of sub- and/or super-synchronous frequency. Due to the active participation of converter controls, the interaction is widely known as the subsynchronous 'control' interaction (SSCI). Note that although the frequency of the 2019 event in the UK's National Grid is below the system's synchronous frequency, careful consideration must be given before characterizing this event as an SSCI event.

Besides SSCI, several high-frequency resonance events have also been reported around the world. For example, the harmonic instability with frequency ranging from 100 Hz to 1 000 Hz in the Borwin1 offshore wind power project in the North Sea of Europe. In 2017, a high-frequency resonance was reported in the Yunnan grid after the Luxi project was put in operation. The high-frequency resonance occurred between the modular multilevel (MMC)-HVDC and the AC grid, triggering the 1 272 Hz and its complementary frequency oscillation. Similar events involving

interactions between converter-based devices and the grid have occurred around the world. The interaction phenomenon causing such high-frequency oscillation is widely known as high-frequency resonance or harmonic resonance.

This technical report aims at revisiting the existing terms and definitions, proposing benchmark models, modeling and analysis methods and mitigation schemes to better understand, analyze and control SSCI.

DYNAMIC CHARACTERISTICS OF INVERTER-BASED RESOURCES IN BULK POWER SYSTEMS –

Part 2: Sub- and super-synchronous control interactions

1 Scope

Based on the interaction phenomenon and frequency range, this part of IEC 63401, which is a technical report, covers the "control interactions" in converter interfaced generators e.g, wind and PV with the frequency of the resulting oscillation below twice the system frequency. SSCI can be categorized into:

1) SSCI in DFIG is caused by the interaction between DFIG wind turbine converter controls and the series compensated network.
2) SSCI involving FSC (both type-4 wind turbine or PV generators) is caused by the interaction between wind turbine or solar PV's FSC controls and weak AC grid.

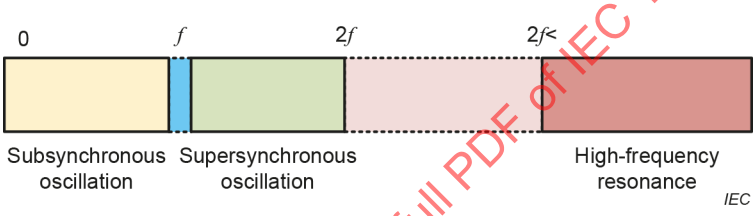

Figure 1 – Multi-frequency oscillations in the modern power system with high-share of renewables and power electronic converters

This technical report is organized into nine clauses. Clause 1 gives a brief introduction and highlights the scope of this document. Clause 4 presents the historical background of various types of subsynchronous oscillation (SSO) and revisits the terminologies, definitions, and classification in the context of classical SSR and emerging SSCI issues to better understand and classify the emerging interaction phenomena. Clause 5 provides the description, mechanism, and characteristics of the SSCI phenomenon in the framework of real-world incidents, including the SSCI events in the ERCOT, Guyuan, and Hami wind power systems. Clause 6 proposes two benchmark models to study the SSCI DFIG and FSC-based wind turbines or PV generators. Clause 7 gives an overview of existing and emerging modeling and stability analysis approaches to investigate the SSCI phenomenon. Clause 8 outlines various techniques to mitigate the SSCI. It discusses various SSCI mitigation schemes, such as bypassing the series capacitor, selective tripping of WTGs, generator, and plant-level damping control schemes. Clause 9 highlights the need for future works towards standardization of terms, definitions, classification, analysis methods, benchmark models, and mitigation methods.

2 Normative references

There are no normative references in this document.

3 Terms and definitions

No terms and definitions are listed in this document.

ISO and IEC maintain terminological databases for use in standardization at the following addresses:

- IEC Electropedia: available at http://www.electropedia.org/
- ISO Online browsing platform: available at http://www.iso.org/obp

4 Terms, definitions and classification

4.1 Existing terms, definitions and historical background

4.1.1 General

This subclause gives a brief overview of the historical developments to define and classify the subsynchronous oscillation issues in traditional power systems. Figure 2 shows a timeline of the classical SSR events and the historical development of terms and definitions related to SSR.

The formation of a series resonance circuit in induction generators in the presence of a series capacitor is not a new phenomenon. This series resonance phenomenon was first observed and named as the induction generator effect (IGE) in 1937 [1][1]. The resonance phenomenon related to the turbine's shaft emerged after the two consecutive resonance incidents that occurred in Mohave generating stations in 1970 and 1971 [2]. The Mohave incidents happened due to the excitation of the shaft's torsional modes, resulting in severe damage to the shafts of the turbo-generators. Post-incident studies on the Mohave incidents led to defining several terminologies for the first time, which have been reported in [3]. The concept of SSR, IGE, torsional interaction (TI) and torque amplification (TA) in a series compensated induction generator was presented. Until this time, SSR was thought to be triggered by the series capacitors in the transmission line. To harmonize the SSR research community, in 1976, a bibliographic report was published by the IEEE in which the work was classified into induction machine effect (IME) and torsional torque oscillation (TTOs) [4]. However, a few years later, another shaft failure event in the Navajo power station revealed that SSR can also be triggered by HVDC converters [5], [6]. Such a phenomenon was later named as the subsynchronous torsional interaction (SSTI) [5]. In an attempt to standardize and redefine the terms, in 1980, the IEEE SSR working group proposed standard definitions of the terms, such as SSR, IGE, TI, and TA to streamline the research community [7]. Subsequently, a second bibliographic supplement was published, which apart from the existing terms/definitions included a new term called device-dependent subsynchronous oscillation (DDSSO). The DDSSO was defined as the oscillation caused by power system devices, such as the power system stabilizers (PSSs) and static var compensators (SVCs) [8]. The SSR field tests at Square Butte showed that the HVDC system was involved in adverse interaction with the shaft of an adjacent turbine generator [9]. Subsequently, the second, third, and fourth supplements to the bibliographic report introduced a new classification in 1985, that is the DDSSO [4], [10], [11].

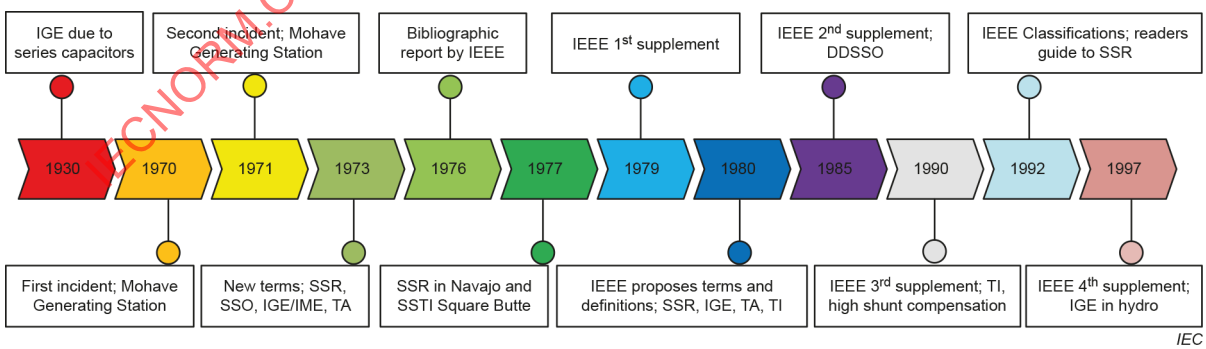

Figure 2 – Timeline of the historical developments of SSO terms, definitions and classification [12]

[1] Numbers in square brackets refer to the Bibliography.

In 1992, the IEEE's working group put forward standard terms to define and classify the SSR issues in conventional turbo-generators [13]. The SSO was divided into SSR and DDSSO. The SSR was further divided into self-excitation (SE), IGE, TI, and shaft TA, as depicted in Figure 3.

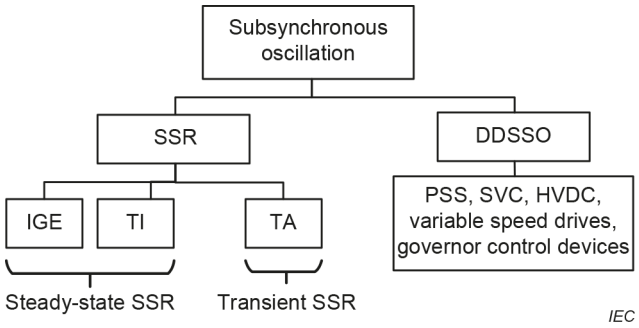

Figure 3 – Terms and classification of SSR by IEEE [13]

4.1.2 Subsynchronous resonance (SSR)

4.1.2.1 General

According to the IEEE definition of the term SSR [13], "it is an electric power system condition where the electric network exchanges energy with a turbine generator at one or more of the natural frequencies of the combined system below the synchronous frequency of the system".

The SSR is further divided into self-excitation (SE), also called steady-state SSR, and transient SSR to include TA. The steady-state SSR or SE covers the SSR caused by IGE and TI [13].

4.1.2.2 Induction generator effect (IGE)

SE of a series compensated induction generator is caused by the IGE, that is when the rotor circuits turn faster than the rotating magnetic field produced by the subsynchronous armature currents. Under this condition, the rotor resistance to subsynchronous current as viewed from the armature terminals becomes negative. The IGE occurs when this negative resistance is more than the sum of the armature and network resistance at a certain subsynchronous frequency [13].

4.1.2.3 Torsional interaction (TI)

TI is the interplay between the mechanical systems (turbine-generator) and a series compensated electrical network. The shaft of the turbine-generator responds to system disturbances at its natural frequencies and produces corresponding subsynchronous voltages at the generator terminals. If this subsynchronous frequency matches with the electrical resonance frequency of the network, the corresponding stator current induces a torque, which excites the torsional oscillations. Each time, the magnitude of the torque increases, resulting in growing oscillations [13].

4.1.2.4 Torque amplification (TA)

TA occurs following a large disturbance in a series capacitor compensated system. The system disturbance causes electromagnetic torque oscillation at the complement of the electrical network's natural frequency. If, somehow, this frequency aligns with one of the natural frequencies of the shaft, a resonance between the network's electrical and shaft's mechanical frequencies occurs [13].

4.1.3 Device dependent SSO (DDSSO)

DDSSO is defined as the oscillation caused by the interaction between turbine generators and a wide range of fast-acting controllers of the power system components, such as HVDC converters, static VAR compensators, and high-speed governor controls.

4.2 Necessity to revisit the terms and classification

The mechanism and characteristics of the SSO associated with the WTGs are quite different from the previously reported conventional SSR events involving turbine generators. For example, the mechanism and characteristics of the interaction phenomenon depend on the structure and parameters of the wind turbine or PV's converter control, which actively participates in the interaction. Furthermore, the SSCI in converter-based generators is not just related to the converter controls; it is rather a system-level issue that is also influenced by other system-wide parameters. The parameters influencing the mechanism and features of the oscillation include wind speed, number of online WTGs, wind turbine converter controls, and their parameters, degree of series compensation, network topology, and stiffness of the AC grid. Another key difference is that the frequency coupling is sometimes very strong, which leads to a very large supersynchronous oscillation component in addition to the subsynchronous component. The frequency coupling effect is obvious in full-converter WTGs, in which sometimes, the magnitude of the supersynchronous oscillation is even larger than the subsynchronous oscillation. These characteristics are very different from the characteristics of SSR in turbo-generators. Thus, the terms, definitions, and classification should be redefined to better understand the mechanism of SSCI in WTGs.

4.3 Revisiting the terms and classification

4.3.1 General

It is recommended that the term "subsynchronous oscillation or SSO" should be used as a general term for an "oscillation" caused by any phenomenon that results in the "oscillation" with its frequency being within the sub-/super-synchronous range. Thus, the SSR, SSCI, IGE, TI, TA and DDSSO should be considered as "phenomena" whereas the "subsynchronous oscillation" as the cause of this phenomenon.

In an electric power system, the subsynchronous interaction phenomena can be better understood by categorizing the contributive system components into the "base" and "interactive" components [12], where

- Base components are the system components that are prone to be interacted by other system components present in the power system;
- Interactive components are the system components that have the potential to initiate or trigger the interaction.

Figure 4 shows a bunch of base and interactive components in a typical power system, that could potentially interact with each other and trigger oscillation in the range of sub-/ super-synchronous frequency. Based on the origin, the subsynchronous interactions can be classified into: 1) torsional interaction, 2) network resonance, and 3) control interaction, as illustrated in Figure 5. The revisited terms and classification are valid for the subsynchronous interaction in both conventional and renewable generations.

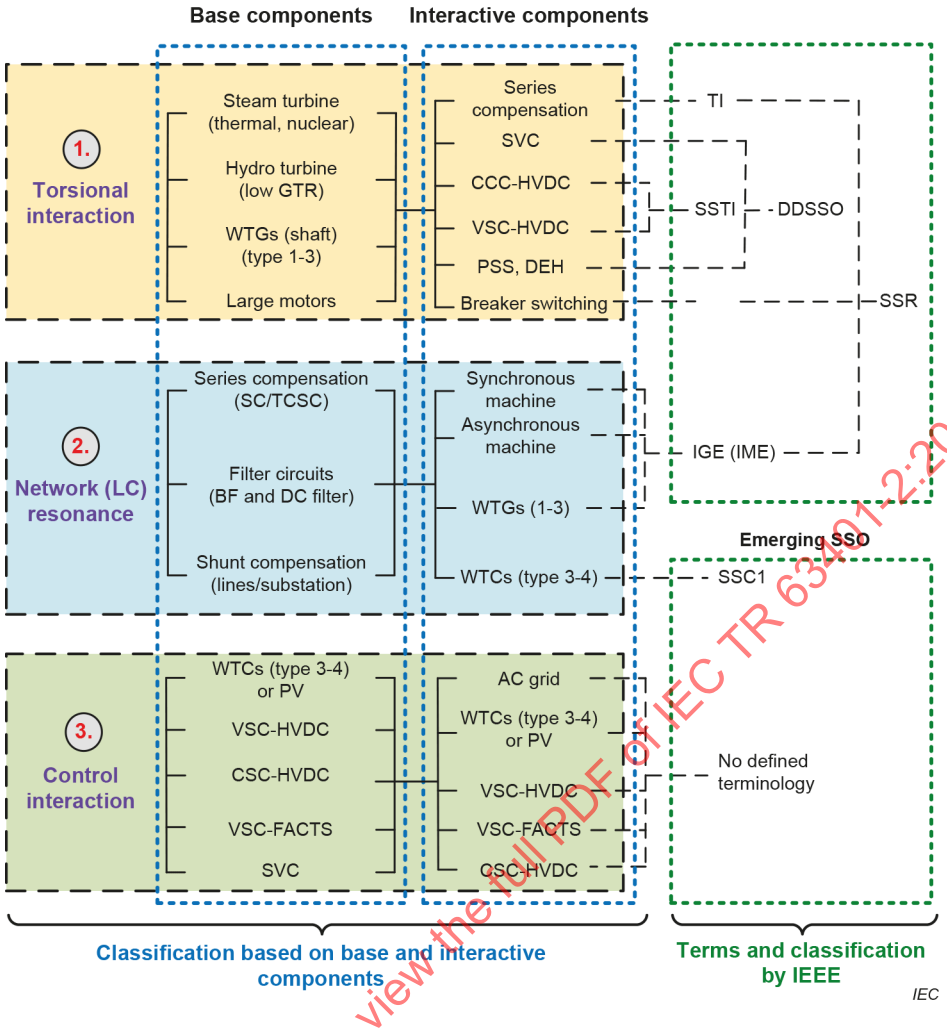

Figure 4 – Classification of subsynchronous interaction based on the origin [12]

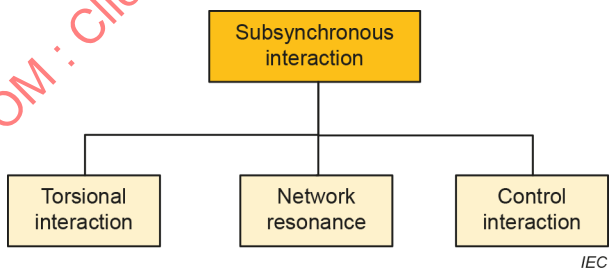

Figure 5 – Reclassification of subsynchronous interactions based on the interaction mechanism

4.3.2 Torsional interaction

The torsional interaction is defined as the interaction in which the mechanical dynamics of the generator shafts (either turbine generator or wind generators) interact with the converter controls of power electronic devices, such as the HVDC, and FACTS.

Referring to Figure 4, the torsional interaction can occur due to the interaction between the mechanical dynamics of any of the base components (such as traditional steam turbines, hydro turbines with low generator turbine ratio, type 1 to 3 wind turbines, and large motors) interact with any of the interactive components (such as fixed series compensation (SC), HVDC converter, FACTS converter, power system stabilizers (PSSs), governor controls, and breaker switching). This type of interaction covers all types of subsynchronous oscillations involving the

shaft dynamics of conventional turbine generators as well as WTGs. It covers the shaft/torsional-related terms proposed in the IEEE's reader guide. The shaft or torsional dynamics terms by the IEEE are TI, TA, and SSTI.

The frequency of oscillation caused by the torsional interaction is in the range of subsynchronous frequency (f_r<f_0), where f_r is oscillation frequency and f_0 is the system's fundamental frequency.

4.3.3 Network resonance

The network resonance is defined as an electric power system condition where a series compensated electric network exchanges energy with the induction generators (either turbo or wind generators) at one or more of the natural frequencies of the combined system below the synchronous frequency. The definition is a modified form of the classical SSR definition.

The network resonance occurs between physically installed inductive (L) and capacitive (C) elements in the generation and transmission sides. The network resonance can also be called the L-C resonance. According to Figure 4, the base components include SC thyristor-controlled series capacitor (TCSC), blocking filter (BF), DC filter, and shunt compensation. The base components can interact with any of the interactive components including synchronous machines, asynchronous machines, WTGs (type 1 to 3), and wind turbine converters (type 3 to 4). The L-C oscillation includes the oscillation phenomenon defined as IGE/IME in the IEEE's classification.

The frequency of oscillation caused by the network resonance lies in the range of subsynchronous frequency (f_r<f_0), where f_r is oscillation frequency and f_0 is the system's fundamental frequency.

4.3.4 Control interaction

The control interaction is the interaction between power electronic converter (PV or wind turbine converter) controls and series compensated or weak AC network. The converter controls in this type of interaction play a key role in defining the mechanism and characteristics of the oscillation.

The basic principle of this type of interaction is similar to the network resonance or L-C oscillation; except that the interaction is between virtual capacitance/inductance offered by power electronic converters controls instead of physical capacitive and inductive elements. According to Figure 4, the base components include wind turbine converters (type 3 to 4) or PV, voltage/current-source converter (VSC/CSC)-based HVDC, or FACTS) devices such as static series compensator (SSSC), static compensator (STATCOM). These base components could be interacted by the interactive components such as weak AC grid, wind turbine converters (type 3 to 4), VSC-HVDC, CSC-HVDC, and VSC-based FACTS controllers. This type of oscillation cannot be explained with IEEE's existing terms.

The frequency of oscillation caused by the control interaction lies in the range of subsynchronous and/or supersynchronous frequency (f_r<f_0 and/or f_0<f_r<2f_0), where f_r is oscillation frequency and f_0 is the system's fundamental frequency.

Besides the above three types of interaction phenomena, the network resonance, torsional interaction, and control interaction can exist simultaneously in a practical power system. The co-existence phenomenon has been observed in the recent real-world events in Guyuan and Hami wind power systems, for example:

- The network resonance and control interaction co-existed in the Guyuan incident. The SSO was triggered by the network resonance and sustained by the control interaction.

- The control interaction and torsional interaction co-existed in the Hami wind power system. The oscillation was initiated by the control interaction and propagated through the grid, which caused the torsional interaction with the nearby turbo-generators.

4.4 Clause summary

The modern power system with high penetration of converter-based renewable power generators faces emerging instability challenges, including the SSCI in converter-based WTGs. The existing terms, definitions, and classification are revisited to accommodate the emerging oscillation issues as indicated by the historical background. In a proposed classification, the subsynchronous interactions are divided into 1) torsional interaction, 2) network or LC resonance, 3) control interaction based on the interaction phenomena.

5 SSCI incidents in real-world wind power systems

5.1 General

In the past decade, several SSCI incidents have occurred in wind power systems around the world [12]. The timeline in Figure 6 shows various SSCI events that occurred around the world. The first event occurred in the XcelEnergy wind power system in Minnesota, USA in 2007 [14], [15]. The incident occurred when the DFIG-wind farms were left in radial connection with the nearby series-compensated transmission line, increasing the net series compensation level. The event caused 9 Hz to 13 Hz SSO. In 2009, a similar SSCI event was observed in the ERCOT wind power system in Texas USA, which caused severe damage to the series capacitors and crowbar circuits [16] to [19]. It was also triggered when the DFIG-wind farms were left in radial connection with the series compensated network, increasing the net series compensation level. The 2009-ERCOT event caused 20 Hz to 30 Hz SSO. In 2011, a 4 Hz SSO event occurred due to the interaction between FSC wind turbines and low short circuit ratio (SCR) caused by the transmission outage in the same system in Texas, USA [20], [21]. From 2012 to 2016, several interactions have been reported in the Guyuan wind power system, causing 6 Hz to 9 Hz SSO [22], [23]. The SSCI occurred when power generated by the DFIG based wind power plant was very low. In 2014 and 2015, the SSCI occurred due to FSC wind turbines connected to the weak AC grid. The triggered SSO matched with nearby thermal power generators and triggered severe torsional oscillation. In 2017, the ERCOT wind power system in Texas faced several oscillation events due to the outage of transmission lines, leaving the wind farms in radial connection. The incidents have been replicated in [24]. In 2019, Great Britain's National Grid experienced a significant power outage [25]. The post-event investigations showed that the converter controls of the Hornsea's offshore FSC wind turbines participated in the event.

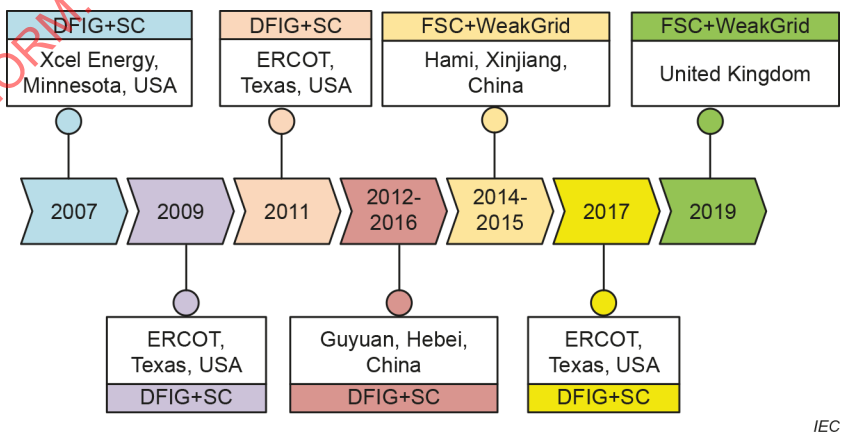

Figure 6 – Timeline of SSCI events reported around the world

The above events can be broadly organized into two types of interactions: 1) the interaction between DFIG and series compensated network, and 2) the interaction between FSC based generators (e.g. type-4 wind turbine and PV) and weak AC network. The active participation of

wind turbine converter "controls" is the key to both types of interactions. Thus, they can be referred to as the "control interactions" or more precisely the "subsynchronous control interactions or SSCI". The "control interaction" can also be caused by the controls of other power electronic devices, such as FACTS and HVDC converters [26]. However, in this document, the term "SSCI" is used to describe the interaction phenomenon involving wind turbine or PV converter controls in the presence of either a series-compensated or weak AC grid. In the following subsections, the prominent real-world SSCI events in DFIG/FSC wind turbines and their mechanisms and characteristics are discussed.

5.2 SSCI in DFIGs connected to series-compensated networks

5.2.1 ERCOT SSCI incident in 2009

5.2.1.1 System description

At the time of the SSCI event, the South Texas transmission network consisted of two 50 % series compensated transmission lines connecting Lon Hill with Edinburg (LH-EB) and Nelson Sharpe with Rio Hondo (NS-RH), as shown in Figure 7. The wind power generated from the DFIG wind farms is fed into the grid through the Ajo substation, located at the middle of the NS-RH line.

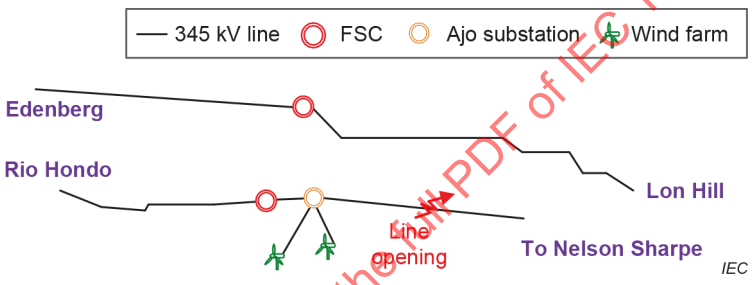

Figure 7 – Structure of the ERCOT wind power system in 2009 [16]

5.2.1.2 Event details

In 2009, an SSCI event occurred when the 345 kV Ajo-LH line was tripped due to a line to ground fault, which eventually left the wind farms in radial connection with the rest of the South Texas grid [16]. The tripping of the AJ-LH line resulted in a sudden increase in the degree of series compensation from 50 % to 75 %, which quickly triggered the oscillation with the oscillation frequency of around 20 Hz to 30 Hz. The recorded current and voltage waveforms are shown in Figure 8. It can be observed that the amplitude of oscillation increased quickly. The post-fault analysis showed that at subsynchronous frequencies, the rotor's negative resistance significantly increased by the participation of WTG's converter controls as seen from the stator terminals. The interaction was indeed triggered by the active participation of the wind turbine converter counters.

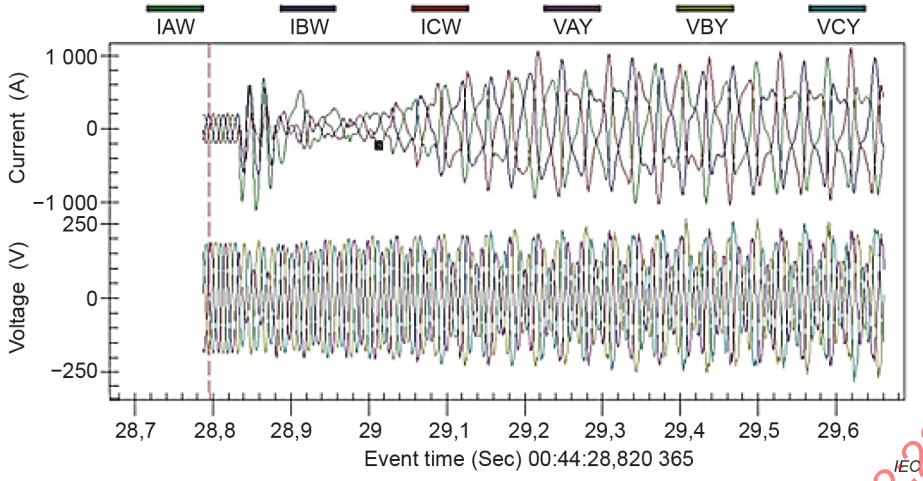

Figure 8 – Oscilloscope record of the 2009 SSCI event in the ERCOT system [19]

5.2.1.3 Consequences

The initiation and build-up process of the oscillation caused by the SSCI was very fast. The amplitude of the system voltages increased to 150 % within 150 ms. The sudden increase in current and voltages damaged the series capacitors and the DFIG's crowbar circuits [19].

5.2.2 ERCOT SSCI events in 2017

5.2.2.1 System description

The one-line diagram of the relevant part of the ERCOT system in 2017 is shown in Figure 9. There are a total of six DFIG-based farms connected with the Lon-Hill Edinburg (LH-EB) 345kV line. Two of the wind farms are connected at substation 3, two at substation 4, and two at substation 5. The transmission line section connecting substations 3 and 4 consists of two series capacitor banks at both ends. It is obvious from the system topology that tripping of the transmission line from either side of the wind power plants would leave the wind farms radially connected to the rest of the network, as shown in Figure 9. In 2017, three SSCI events were detected, which were triggered by the transmission line outages.

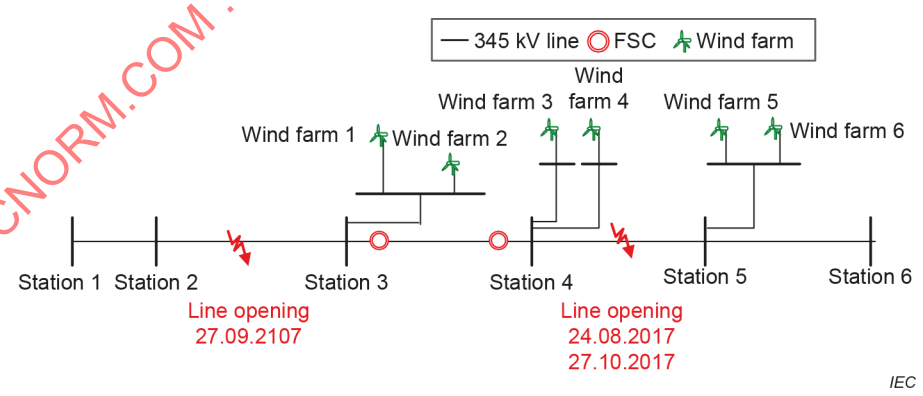

Figure 9 – Structure of the ERCOT wind power system in 2017 [24]

5.2.2.2 Event details and consequences

In 2017, three SSCI events were recorded in the ERCOT system in three months [24].

Event#1: The first SSCI event was detected on August 24, 2017. The SSCI was triggered when the 345kV transmission line section connecting substations 4 and 5 tripped due to a transmission line fault. After the 2009 event, the ERCOT system was equipped with an

appropriate protection system to detect the oscillation. Thus, the series capacitors were bypassed automatically when the oscillation was detected by the protection system, which saved the capacitors from being damaged. Twenty minutes later, the series capacitors were brought into service manually. However, the SSCI triggered again and the magnitude of the oscillation increased rapidly. The recorded current and voltage waveforms along with the frequency spectrum before and after the capacitor reinsertion are shown in Figure 10. The oscillation disappeared after the series capacitor was bypassed.

Event#2: The second SSCI event was recorded on September 24, 2017. A line-to-ground fault between substations 2 and 3 left the wind farms 1 and 2 to operate with the two series capacitors, as indicated in Figure 9. The diverging oscillation suddenly appeared in the current signal. Consequently, wind farms 1 and 2 were tripped within 24 cycles, by the differential protection relay of the step-up transformer. The recorded current and voltage waveforms are shown in Figure 11.

Event#3: The third SSCI event was observed on October 27, 2017. In this event, a line to ground fault between substations 4 and 5. The line opening caused the wind farms 3 and 4 to operate with the two series capacitors installed between the substation 3 and 4. Compared to the August 24 event, a less intense oscillation was excited. The oscillation disappeared after the faulty line section was manually restored within three minutes. The SSCI event was less severe and the series capacitors were not damaged, nor the wind power plants tripped. The recorded current, voltage, and frequency spectrum are given in Figure 12.

In all three events, the SSCI occurred when the wind power plants formed a radial connection with the series capacitors. The frequency of the resulting oscillation remained within the subsynchronous frequency range 20 Hz to 30 Hz. The magnitude of the corresponding supersynchronous frequency components was negligible in all three events.

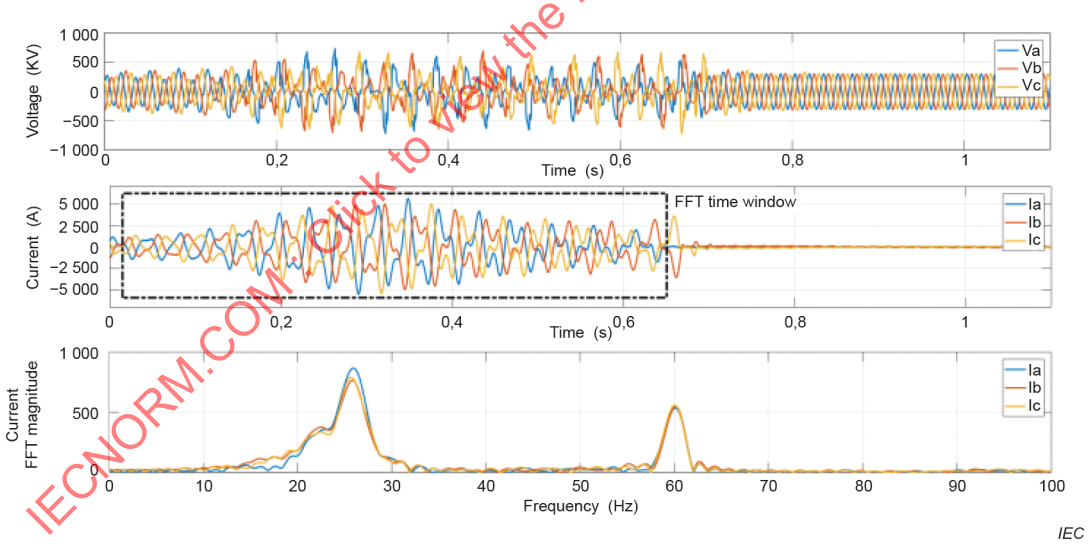

Figure 10 – Event#1 August 24, 2017: current, voltage and frequency spectrum of the current during the SSCI event and after bypassing the series capacitor [24]

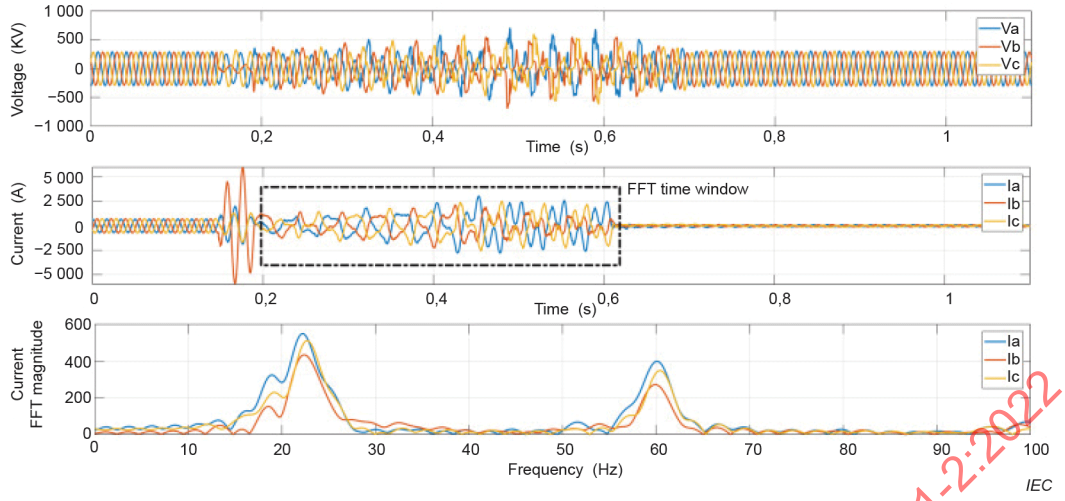

Figure 11 – Event#2 September 27, 2017: current, voltage and frequency spectrum of the current during the SSCI event [24]

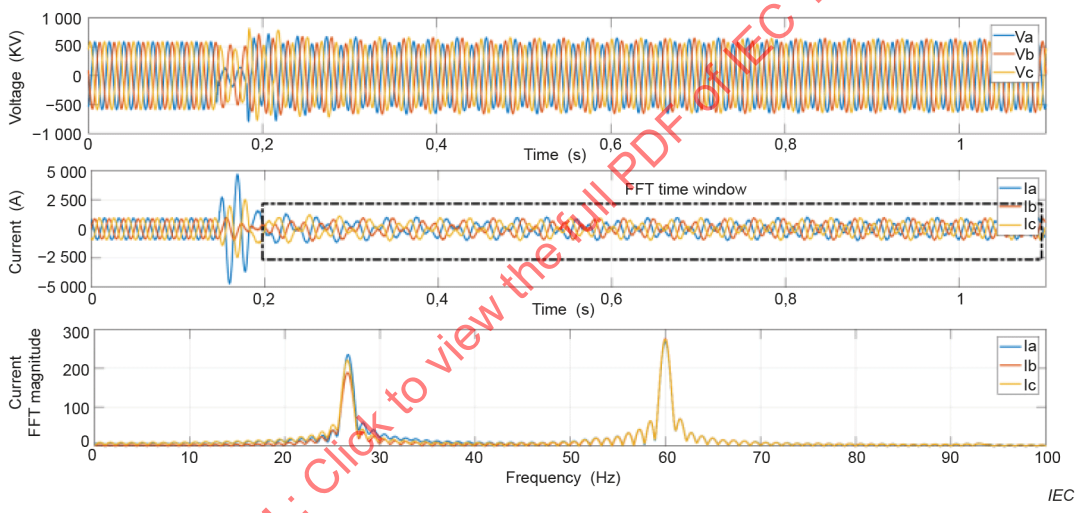

Figure 12 – Event#3 October 27, 2017: current, voltage and frequency spectrum of the current during the SSCI event [24]

5.2.3 SSCI events in Guyuan wind power system

5.2.3.1 System description

The Guyuan wind power system is located in the northwest of Hebei Province, China. The geographical layout of the wind farms and the series compensated transmission lines in the Guyuan system is shown in Figure 13. There are twenty-four wind farms in the Guyuan area – with an installed capacity of 4224 MW. In the whole wind power plant, there are three types of WTGs, including DFIG, FSC wind turbine, and self-excited induction generator (SEIG) with the proportions of 82,8 %, 15,4 %, and 1,8 % respectively. Most of the wind farms are homogenous, meaning that they contain only one type of WTG. Each wind farm in the Guyuan area is radially connected to the corresponding 220 kV substations. The substations are Beilonghshan, Yiyuan, Chabei, Lianhuatan, and Hengtai, as shown in Figure 13. The power from the 220 kV substations is collected at the 500 kV Guyuan substation through a 220 kV/500 kV power transformer. The Guyuan substation connects the Hanhai and Taiping regions through double-circuit parallel transmission lines. The transmission lines connecting Hanhai with Guyuan and Guyuan with Haiping are referred to as Guyuan-Hanhai and Guyuan-Taiping, respectively. There are a total of four series capacitor banks installed at the double circuit Guyuan-Hanhai and Guyuan-Taiping with the compensation degrees of 40 % and 45 %, respectively.

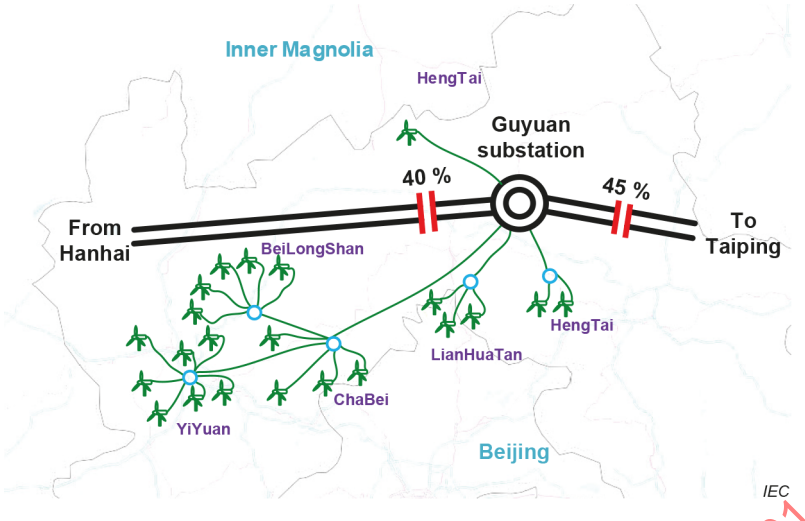

Figure 13 – Geographical layout of the Guyuan wind power system, Hebei Province, China

5.2.3.2 Event details

The series capacitors in the Guyuan system were commissioned in October 2010 to enhance the power transfer capability of the Guyuan-Taiping and Guyuan-Hanhai transmission lines. Since then the Guyuan wind power system has been facing severe SSCI incidents. The SSCI occurs under the condition that all the series capacitors of the 500 kV double circuit lines are in operation and the wind farms are operating normally. The SSCI phenomenon disappears when one of the four series capacitors is bypassed. In December 2012, more wind farms were installed in the Guyuan area. The increased proportion of wind farms led to more frequent SSCI issues. During December 2012 and December 2013, as many as fifty-eight SSCI events were detected. Here, only one SSCI incident is discussed because the mechanism and characters of most of the SSCI events are identical. For one of the fifty-eight events, the active power flow recorded at the 220 kV side of the Guyuan transformer is plotted in Figure 14. When the SSCI occurred, a diverging oscillation emerged at 14:12:0. The magnitude of the oscillation quickly increased. Consequently, when the oscillation is detected by the protection system, hundreds of WTGs tripped within 30 s and the total generated power decreased dramatically. The reduced number of ins-service WTGs resulted in positive damping at the subsynchronous frequency and the oscillation gradually damped or converged. Although the oscillation was damped to some extent, the SSCI still existed until one of the series capacitors was brought out of service at 14:14:3.0, as seen in Figure 14. The corresponding single-phase current and voltage waveforms recorded at the 220kV substation are shown in Figure 15 and Figure 16, respectively. It is evident from Figure 15(a) that the current waveform during the SSCI event has a large subsynchronous component. The frequency spectrum of the current in Figure 15(b) shows that the frequency of the oscillation is 8,1 Hz. Besides the subsynchronous frequency component, the current waveform also has a large super-synchronous oscillation component of 91,9 Hz. The magnitude of the subsynchronous current was larger than half of the fundamental component, while the magnitude of the supersynchronous component was negligibly small. The measured voltage waveform and its frequency spectrum are shown in Figure 16(a) and (b), respectively.

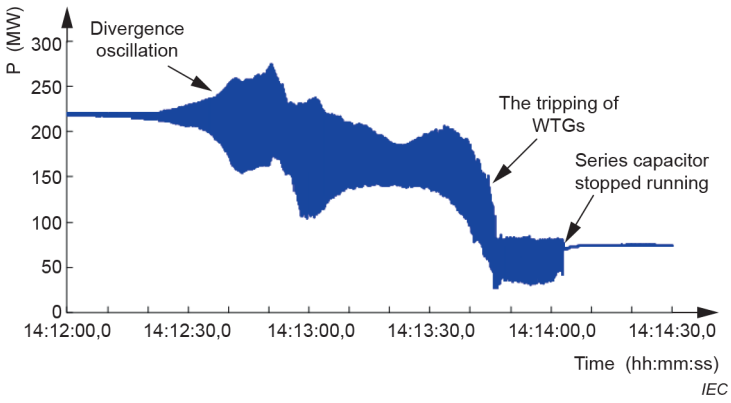

Figure 14 – Power flow measured at the 200 kV side of the Guyuan step-up transformer

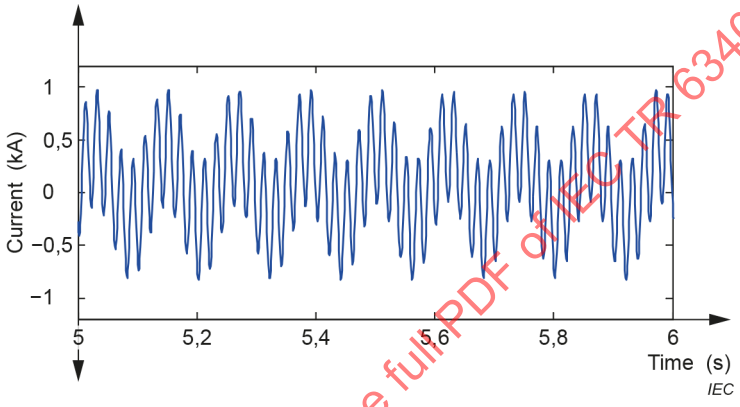

(a) Phase A current

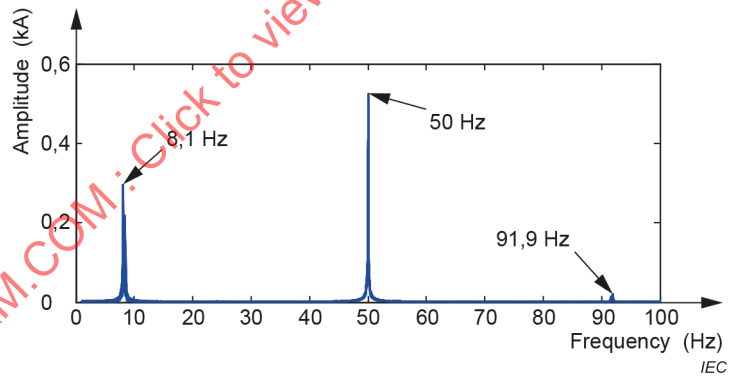

(b) Frequency spectrum of phase A current

Figure 15 – Field recorded line current and frequency spectrum

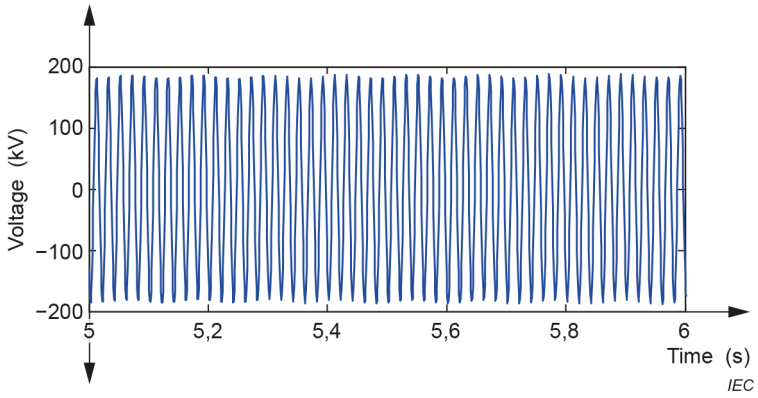

(a) Phase A voltage

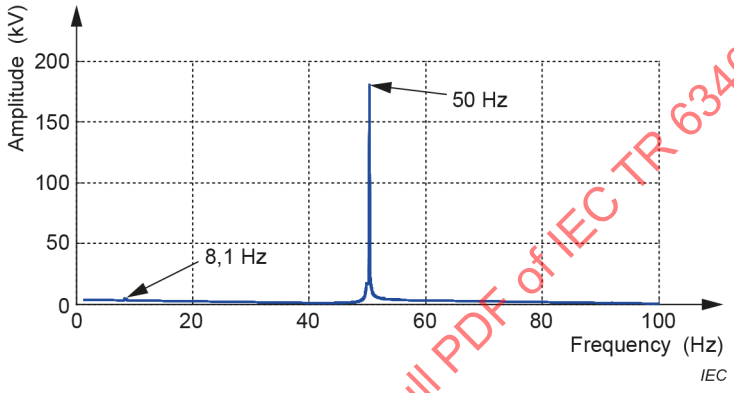

(b) Frequency spectrum

Figure 16 – Field recorded voltage and frequency spectrum

The characteristics of the SSCI events are summarized as follows:

- The SSCI occurs when the power generated by wind farms is small, i.e., the output power does not exceed 13 % of the total installed capacity of wind power.
- For the fifty-eight SSCI events, the oscillation frequency is different for different SSCI events, approximately ranging between 6 Hz and 9 Hz.
- The oscillation frequency during an SSCI event also varies with time due to changes in wind speed and hence the output power level. The frequency decreases as the number of online WTGs decreases.
- The characteristics of the triggered oscillation such as magnitude and frequency depend on the wind speed, the number of in-service WTGs, series compensation, wind turbine converter controls, and their parameters.
- The current amplitude of the FSC-based wind farms in the Guyuan system is much lower than that of the DFIGs-based wind farms. The oscillation originated from the DFIGs due to negative damping at the subsynchronous frequency.
- One of the main differences in the SSCI events in Guyuan and ERCOT is that the SSCI occurs without transmission line faults that leave the WTGs in radial connection with the grid. The SSCI is triggered at certain operating conditions, such as low wind speeds and a small number of in-service DFIGs. In addition, the SSCI events in the Guyuan system are quite frequent. The SSCI events in the ERCOT system were triggered when the equivalent series compensation was increased due to a transmission line outage. Thus the SSCI events were less frequent.

5.2.3.3 Consequences

When the SSCI occurred, the subsynchronous current grew rapidly. Consequently, hundreds of WTGs tripped when the current distortions exceeded the preset threshold. This resulted in a

sudden decrease in wind power being sent to the grid. The frequent decline in wind power seriously threatens the safe and stable operation of the Guyuan wind power system. Besides the loss of power, the vibrations and loud noise in the substation transformers speed up the aging of transformer insulation or can even damage the transformers, which makes the system less reliable.

5.3 SSCI in FSC-based generators connected to weak AC network

5.3.1 SSCI event in Hami wind power system

5.3.1.1 System description

The Hami wind power system is located in the Xinjiang Autonomous Region of China. It consists of several DFIG and FSC wind turbine clusters. The geographical layout of the Hami system and the relevant portion of the nearby generators and regional loads is shown in Figure 17. The power generated by the wind farms is collected at substations A, B, and C. It is then transmitted to substation D through 109 km and 134 km long transmission lines. The accumulated power is fed to the main 750 kV grid through a 220 kV double circuit transmission line. The grid-station H is connected with the thermal power plants M (consisting of four 660 MW units) and N (consisting of two 660 MW units), and a ±800 kV HVDC link to transfer the surplus power to the Central China Power Grid. The large number of wind farms located far away from the central grid makes the short circuit ratio smaller, and thus the AC grid becomes weak. The grid connection becomes even weaker, particularly when the generated output power is very low because of low wind speeds or a smaller number of in-service WTGs.

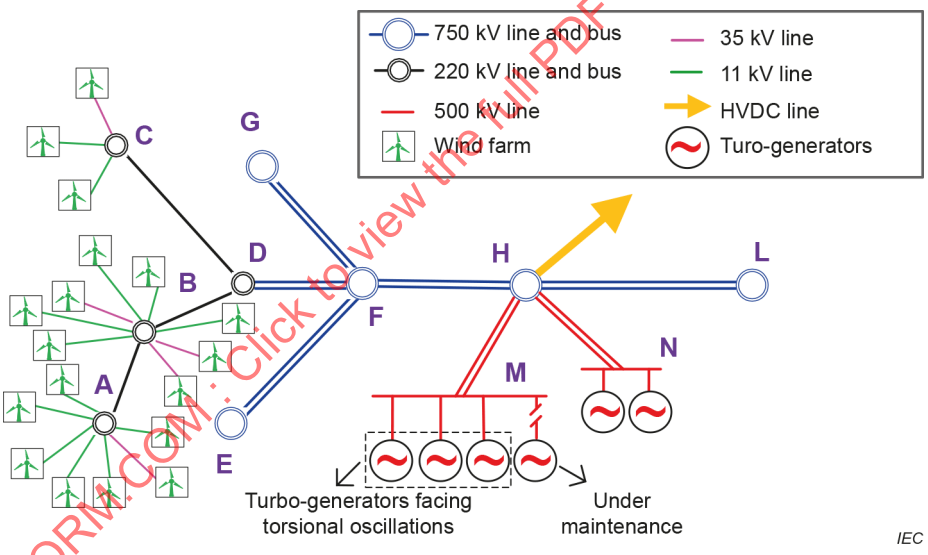

Figure 17 – Hami wind power system, Xinjiang, China [27]

5.3.1.2 The SSCI event

The Hami wind power system faced a severe SSCI incident on July 1, 2015 [27]. The post-fault analysis demonstrated that the oscillation originated from FSC wind turbines and spread in the whole central grid having a low short circuit ratio. The measured phase A current and active power show strong sub- and super-synchronous oscillation components, as shown in Figure 18. The current and power waveforms are severely distorted due to the very high magnitude of the oscillations. The corresponding frequency spectrums of the current and active power are obtained with a window length of 10s and are given in Figure 19. The magnitude of the subsynchronous component is slightly less than the fundamental component while the magnitude of the supersynchronous component is higher than the fundamental.

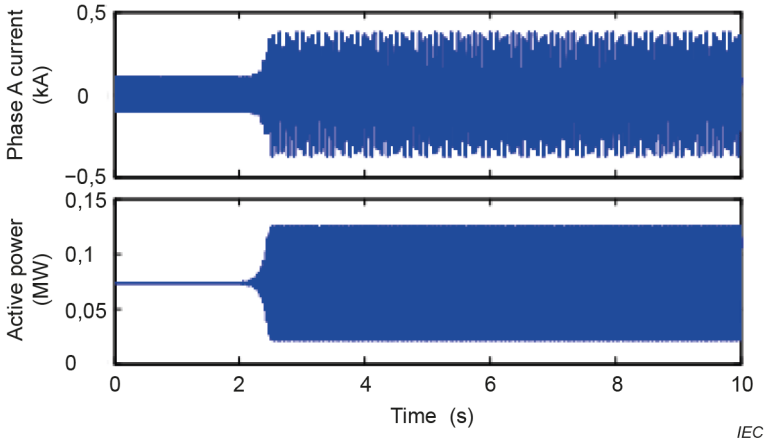

Figure 18 – Current (upper plot) and active power (lower plot)

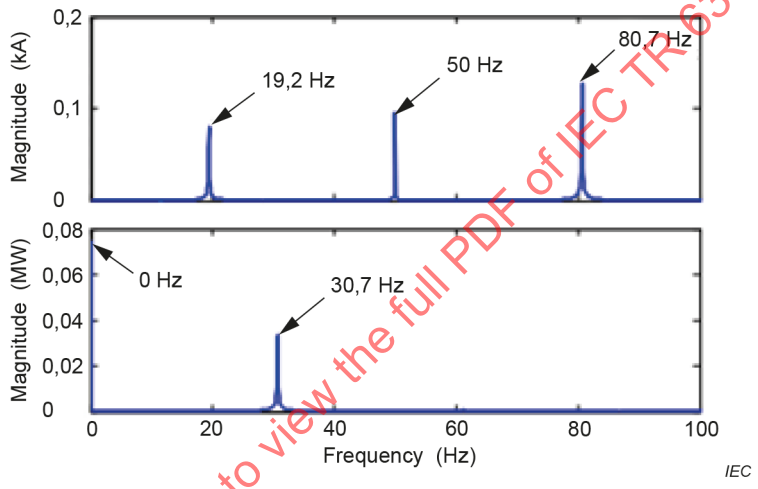

Figure 19 – Frequency spectrum of the current (upper plot) and active power (lower plot)

The nearby thermal power plants are represented by M and N. Unfortunately, the frequency of triggered oscillation matched with the torsional frequencies of these thermal generators, which triggered a strong torsional vibration in the shafts of the turbo-generator unit #1, #2, and #3. Eventually, the torsional relays tripped the turbo-generators and the power transfer, thereby dropping the power transfer in the HVDC link from 4 500 MW to 3 000 MW. The field recorded active powers of the actual incident are shown in Figure 20. The frequency matching of the turbogenerator oscillation modes and frequency of SSO is illustrated in Figure 21.

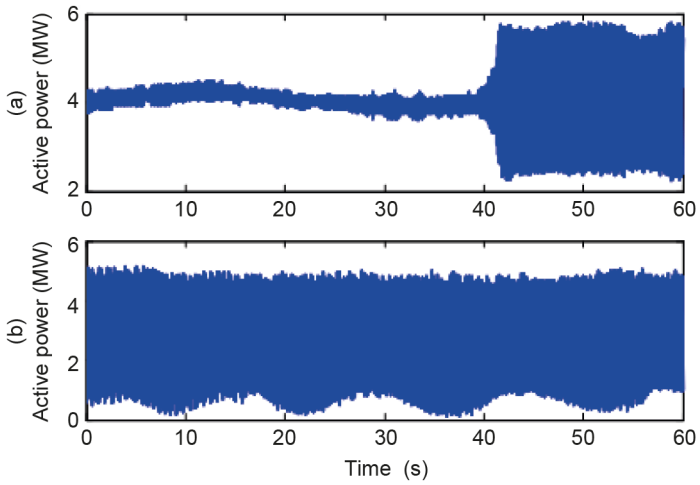

Figure 20 – Field measured active power of a wind farm (a) From 09:46 to 09:47 (b) From 11:52 to 11:53

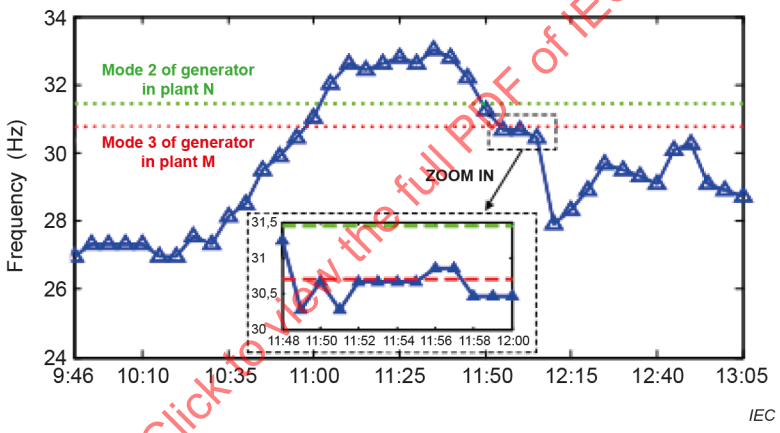

Figure 21 – Torsional modes and frequency variation of the unstable oscillation

5.3.1.3 Consequences

The post-fault analysis on the data recorded from phasor measurement units / wide-area measurement system (PMUs/WAMS) showed that the direction of subsynchronous power is from substations A/B/C to the power plant M, through grid-stations D, F, and H [28]. Moreover, it was found that the power flow from HVDC to grid-station H was quite low (almost zero), meaning the HVDC converters did not participate in the interaction. Essentially, the oscillation was caused by the interaction between the weak AC grid and the FSC- based wind farms. Besides, it has also been found that the FSC's controls actively participate and play a key role in defining the characteristics of the interaction. The SSCI event lasted for 300 minutes and the oscillation frequency during the event varied between 27 Hz to 33 Hz, as shown in Figure 21. The frequency matching with the natural frequency of the shaft modes can cause torsional stress on the shaft. As a result, the tripping of turbo-generators by their torsional relays resulted in the loss of generated power. The effect of generator tripping on their natural oscillation modes is depicted in Figure 22.

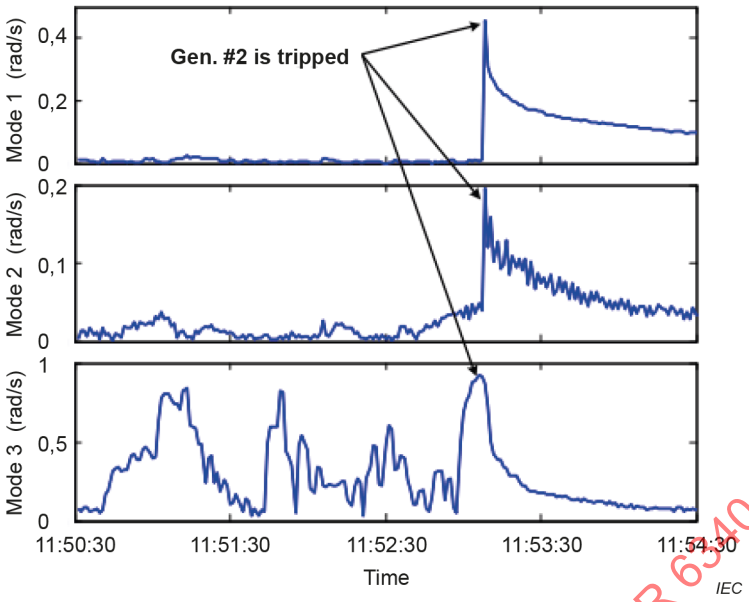

Figure 22 – Torsional speed of modes 1 to 3 of unit #2 in Plant M

5.4 Clause summary

This clause overviewed the most prominent real-world SSCI events in wind power systems around the world. The interaction mechanism and consequences of each event are discussed. The SSCI in DFIGs connected to a series-compensated network triggers oscillation at the subsynchronous frequency and the frequency coupling effect is not strong. The SSCI in FSC connected to a weak AC grid leads to both sub- and super-synchronous frequency due to the strong frequency coupling effect. The participation of wind turbine converter controls is common in either type of interaction. The characteristics of the interaction phenomena are significantly influenced by system-wide parameters and operating conditions in both network and generation sides. A summary of the SSCI events in various wind power systems is presented in Table 1.

Table 1 – Comparison of the characteristics of real-world SSCI events

Event	WG type	Frequency	Grid	Causes	Characteristics	Consequences
ERCOT, Texas	DFIG	20 Hz to 30 Hz	Series compensation, triggered by transmission line outage	Interaction between DFIG converter controls and series compensated transmission line	Fast initiation and build-up process, Time-varying oscillation frequency	Damage to the series capacitors and turbine's crowbar circuits
Guyuan, Hebei	DFIG	6 Hz to 9 Hz	Very low series compensation level, triggered by capacitor switching and/or output power level	Interaction between DFIG converter control and series compensated network	Time-varying oscillation frequency, induction generator effect (IGE) and SSCI co-exit	Significant loss of power, stability and reliability issues
Hami, Xinjiang	FSC wind turbine	27 Hz to 33 Hz	Weak grid connection	Interaction between FSC control and weak AC grid	Time-varying oscillation frequency	Significant loss of power, torsional stress

6 Modeling and analysis approaches

6.1 Preview

Several modeling and analysis methods have been used to investigate the SSCI phenomenon and characteristics. Based on the analysis domain, the modeling and analysis approaches can be classified into 1) time-domain modeling and analysis approaches, and 2) frequency-domain modeling and analysis approaches. The modeling and stability analysis methods include the classical approaches, which have been utilized for the classic SSR studies in turbo-generators, and the emerging approaches developed during the past decade, e.g., the small-signal impedance modeling and analysis approaches, which are more suitable for the SSCI related studies [29]. This section will discuss only those modeling and analysis methods that have been widely used for investigating the SSCI. However, in addition to the modeling methods mentioned here, there have been efforts on empirical modelling (or generic multi-frequency modeling) on converter-systems, which can also be used for SSCI studies.

6.2 Time-domain modeling and analysis approaches

6.2.1 General

Time-domain modeling analysis approaches include nonlinear time-domain electromagnetic transient (EMT) simulation, hardware-in-the-loop simulation, and linearized state-space modeling and modal analysis. This clause discusses the technical requirements, strengths, and weaknesses of each method for SSCI studies.

6.2.2 Nonlinear time-domain EMT simulation

The time-domain EMT simulations are based on the EMT models of the actual system components. The EMT models include enough details for reproducing the dynamics on a time scale according to the electromagnetic phenomena. EMT models can represent the dynamics of power electronic converters and their control systems. EMT modeling and analysis is a common and widely used method for studying the control participated oscillatory instabilities. In order to carry out EMT analysis for SSCI studies, a validated and verified EMT model provided by the original equipment manufacturer should be used. It is recommended that the standard default models available in the built-in libraries of EMT software should not be used.

The EMT simulations are important as they are generally used to confirm the analysis results obtained from other methods, for instance, eigenvalue, impedance modeling and analysis, complex torque analysis, and frequency scan analysis. Once the equivalent EMT simulation model of an actual system has been established, it is easy to perform various studies and check the system's behavior under different operating conditions and contingencies.

The importance of power system analysis using validated/benchmarked and verified user/OEM EMT models cannot be under-emphasized. In Australia for example, the entire transmission network has been modeled in EMT due to the pervasive and rapid uptake of large-scale transmission connected converter-based renewable generation.

The EMT simulations require a very small simulation time step to study sub- and super-synchronous frequency dynamics, which could result in a heavy computational burden. The EMT simulation of a normally large-sized power system can take several hours. Another major limitation of the EMT simulation-based analysis is that all the mechanical and electrical parameters of the system components are required to replicate the actual system into a simulation model. Sometimes, the control structures and parameters of the converter based devices are not available.

6.2.3 Controller hardware-in-the-loop simulation

The SSCI is a 'control interaction' phenomenon. The dynamics of the 'wind turbine converter controls' significantly impact the mechanism of the SSCI. The hardware simulators allow real-time simulations by interfacing the physical wind turbine converter 'controllers' with the rest of

the software simulation model under realistic operating conditions. Both, the software and hardware parts of the simulation are simulated in real-time, called the controller controller-hardware-in-the-loop (CHIL) simulation.

Figure 23 shows the configuration of a typical CHIL simulation platform for a DFIG-based wind power system. The DFIG, wind turbine converter controller and hardware simulator are connected by input-output (IO) boards to form a closed-loop test system. The hardware part includes the wind turbine converter controllers, the main controller, the hardware simulator, and a user workstation. The software part includes the simulation model of the wind power system (DFIGs, grid, transmission lines, etc.), which are developed in an EMT software, depending on the real-time simulator. The operation, control, and protection strategy of WTG consist of two parts. One is provided by the main control and the other is by its converter controller. The hardware simulator and the WTG controller are interfaced through the analog/digital signals. The simulation results for various parameters can be viewed and analyzed through the workstation software to determine the system's stability at various operating conditions.

One of the countermeasures for mitigating the SSCI is to modify the WTG's converter controls, for example, adjusting the wind turbine converter control parameters or supplementing the wind turbine converter controllers with damping control loops [30]. The CHIL simulations are important to check the damping performance and to investigate the impact of wind turbine converter control modifications on the WTG's dynamic and low-voltage ride-through (LVRT) performance, before implementing the modified wind turbine converter controls in actual WTGs. The hardware equipment required for the CHIL simulations is expensive.

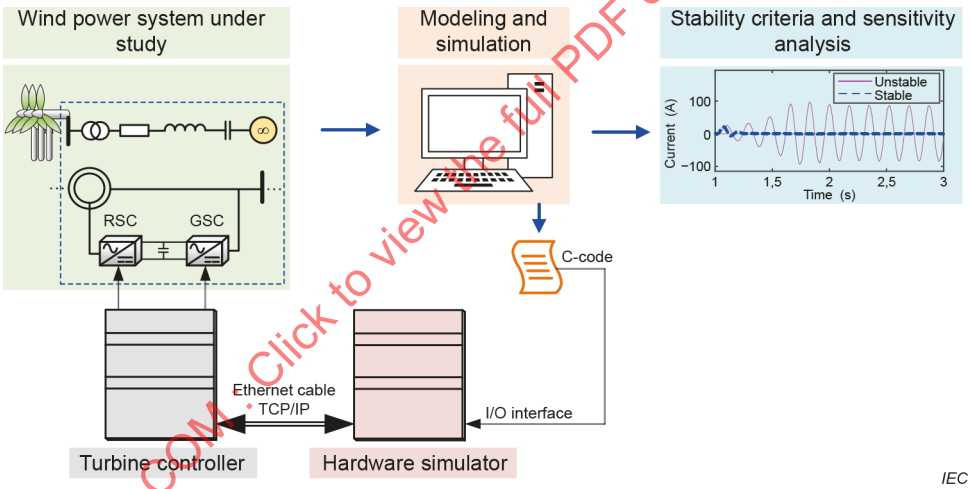

Figure 23 – Configuration of CHIL simulation

6.2.4 Linearized state-space modeling and modal analysis

Modal analysis is an effective and accurate method that provides valuable information about the dynamic stability of the power system. It is suitable for the analysis of various types of SSO issues except for transient TA. The accuracy of the calculation results depends on the accuracy of the parameterized models of the dynamic components of the system. The application of modal analysis in the study of SSCI stability consists of the following three steps:

1) First, the state-space model of the system is established and linearized to obtain the state-space matrices;
2) Then, the eigenvalues of the system are solved according to the state-space matrices. After that, the damping and frequency information of all oscillation modes are obtained, and the dominant and oscillation modes with the lowest damping are identified.
3) Finally, solve the eigenvectors and the participation factors of the dominant oscillation mode, and get the participation degree of the dynamic components of the system to the mode (optional).

The details of the above three steps can be found in [31], [32].

6.2.5 Discussions on time-domain approaches for SSCI studies

The features, advantages, and disadvantages of the time-domain approaches for SSCI studies are presented in Table 2.

Table 2 – Main Features of time-domain approaches for SSCI studies

Method	Features	Advantages	Disadvantages
EMT simulation	Software-based simulations Includes nonlinear loops, and detail electromagnetic transient dynamics	Can be used to validate the results obtained from other stability analysis methods Can be used to check system response at different operating conditions	Lack of theoretical analysis and hard to understand the mechanism behind the phenomena Difficult to find the operating points where the system is unstable Detailed prior information about the system configuration, topologies, and parameters is required
Hardware-in-loop simulation	Combines the hardware and software Can be used to carry out impedance analysis based frequency sweeps and testing mitigation controls	Converter control dynamics can be studied in real-time with controller hardware Real-time simulation can reflect the real circuit dynamics in detail including communication delays, etc.	In addition to the disadvantages of EMT simulations, the hardware equipment for the CHIL simulations is expensive
Linearized state-space modeling and modal analysis	Linearized system based on a specific operating point	Theoretical analysis is useful to understand the mechanism behind the SSCI phenomena	Cannot reflect the impacts of nonlinear factors on the SSCI

6.3 Frequency-domain modeling and analysis approaches

6.3.1 Frequency scanning

Frequency scanning is a traditional frequency domain analysis method that has been used for the classical SSR in turbo-generators. It can also be used to study the SSCI in WTGs. In this method, the equivalent impedance (or damping), as seen from the internal buses of generators looking into the network, is computed for different values of frequency. It gives information about the natural frequencies of the system and the tendency towards SSCI. This approach is particularly suited for the preliminary analysis of SSCI.

The core of the frequency scanning method is to get the impedance-frequency curve of the whole system seen from the internal bus of the generator, including the reactance-frequency curve and the resistance-frequency curve. To obtain the impedance-frequency curve, a series of voltage/current perturbations with different frequencies are injected.

Assume the damping provided by generators is zero. The system is unstable if the system resistance is negative, i.e., $R(f)$ <0 at the oscillation frequencies. On the other hand, the system is stable if the system resistance is positive at the oscillation frequencies.

The frequency scanning method is a cost-effective method to screen out the system conditions that may trigger the SSCI and determine the parts of the system that do not influence the oscillation phenomenon. It is however only an approximate linear method, which can only tell the possible occurrence of an SSCI event. It is suitable for preliminary analysis of the risk of SSCI during the planning and design stages. If the risk of SSCI has been identified by the frequency scanning method, it is necessary to study the detailed characteristics of oscillation

more accurately and quantitatively by other analysis approaches, such as modal or time-domain simulation analysis.

The advantages of the frequency scanning method are summarized as follows:

1) It is an easy, simple, economical, and faster way to check where there is a risk of SSCI or not.
2) It has a clear physical meaning, which can easily be understood by field engineers.

The main disadvantages of this method include:

1) The method just tells the risk of SSCI. If there is a risk of SSR, further detailed analysis is required.
2) The generator model is highly simplified; thus, the influence of the system operation mode and transient characteristics of the controller are not considered.

6.3.2 Complex torque coefficient method

Complex torque coefficient method is an extension of the damping torque analysis in the field of SSO analysis. In this method, the focus of the stability studies extends from the electromechanical oscillation mode of the system to the SSO mode. It is a frequency domain analysis method based on a linearized system model.

On the one hand, based on the linearized equations of the multi-mass shaft system of a turbo-generator set [33], perturbations in the generator rotor angle ($\Delta\delta$), in the Laplace domain, is related to the perturbations in the electrical torque (ΔT_e) by

$$\Delta T_e = -k_m(s)\Delta\delta \tag{1}$$

Where $k_m(s)$ is the mechanical transfer function and s is the Laplace operator. The incremental mechanical torque components are neglected.

On the other hand, considering the electrical system, including that of the generator, the electrical torque ΔT_e can be developed into the function of the generator rotor angle $\Delta\delta$ as

$$\Delta T_e = k_e(s)\Delta\delta \tag{2}$$

Where $k_e(s)$ is the electrical transfer function between ΔT_e and $\Delta\delta$.$k_e(s)$ can also include impacts of various system components/controllers, e.g., the automatic voltage regulator (AVR) and the PSS, on the torsional phenomenon.

Substituting for ΔT_e from (1) in (2), we obtain

$$(k_e(s) + k_m(s))\Delta\delta = 0 \tag{3}$$

The total complex torque coefficient can be expressed as

$$k(j\omega) = k_m(j\omega) + k_e(j\omega) = K(\omega) + j\omega D(\omega) \tag{4}$$

$$\begin{cases} k_{\mathrm{m}}(j\omega) = K_{\mathrm{m}}(\omega) + j\omega D_{\mathrm{m}}(\omega) \\ k_{\mathrm{e}}(j\omega) = K_{\mathrm{e}}(\omega) + j\omega D_{\mathrm{e}}(\omega) \end{cases} \tag{5}$$

where complex torque coefficient of mechanical system $k_{\mathrm{m}}(s)$ is divided into mechanical elastic torque coefficient $K_{\mathrm{m}}(\omega)$ and mechanical damping torque coefficient $D_{\mathrm{m}}(\omega)$, complex torque coefficient of electrical system $k_{\mathrm{e}}(s)$ is divided into electrical elastic torque coefficient $K_{\mathrm{e}}(\omega)$ and electrical damping torque coefficient $D_{\mathrm{e}}(\omega)$ [34].

The system stability criteria are as follows.

1) If $D(\omega)|_{K=0} > 0$, oscillation will not occur (positive damping).
2) If $D(\omega)|_{K=0} = 0$, the system is critically stable(critical damping).
3) If $D(\omega)|_{K=0} < 0$, oscillation will occur (negative damping).

where ω is the angular frequency when the elastic torque coefficient $K_{\mathrm{m}}(\omega)$ equals to zero.

Electrical complex torque coefficient $k_{\mathrm{e}}(j\omega)$ can be derived either from the transfer function model of the system or from the test curve of the physical system or time-domain response curve. The steps of these two approaches to obtain $k_{\mathrm{e}}(j\omega)$ are introduced as follows, respectively.

1) The detailed steps of the complex torque coefficient method based on time-domain simulation are as follows:
   a) Establish and debug the transient simulation model of the system and bring the system to a steady-state condition.
   b) Under the operating conditions to be studied, a small perturbation torque $\Delta T_{\mathrm{m}} = \Sigma\left[T_{\mathrm{a}}\cos\left(\lambda\omega_0 t + \varphi_{\mathrm{i}}\right)\right]$ is applied to the generator rotor, the frequency of ΔT_{m} is $f = \lambda f_0$ ($0 < \lambda < 1$, f_0 is the fundamental frequency), T_{a} is the amplitude of ΔT_{m}, and φ_{i} is the phase of ΔT_{m}.
   c) When the system enters the steady-state again, the electromagnetic torque T_{e}, power angle δ, and speed ω of the generator are intercepted for the same period.
   d) Spectrum decomposition of the above three quantities at each frequency f.
   e) The electric elastic torque coefficient and the electric damping torque coefficient at the excitation frequency are calculated. Then the stability of the system SSO is judged according to the complex torque coefficient stability criteria.
2) The complex torque coefficient of a mechanical system is usually calculated by the transfer function model. The steps of the complex torque coefficient method based on the transfer function are as follows:
   a) The relationship between the total electromagnetic torque variation and the rotor speed can be obtained as

$$\Delta T_{\mathrm{e}}(s) = G_{\mathrm{Te}}(s)\Delta\omega_{\mathrm{r}} \tag{6}$$

Where $G_{\mathrm{Te}}(s)$ is the equivalent electrical transfer function from the generator's rotor speed looking into the network.

b) When the frequency of the rotor speed change is Ω, the gain of the total torque change at this frequency is given as

$$G_{\mathrm{Te}}(j\Omega) = |G_{\mathrm{Te}}|\cos\varphi_{\mathrm{Te}} + j|G_{\mathrm{Te}}|\sin\varphi_{\mathrm{Te}} = G_{\mathrm{Tex}} + jG_{\mathrm{Tey}} \tag{7}$$

where $|G_{\mathrm{Te}}|$ and φ_{Te} represent the amplitude and phase of the total torque at frequency Ω; G_{Tex} and G_{Tey} are the real and imaginary parts of the total torque variation gain, respectively. It is assumed that the initial phase of the rotor speed variation $\Delta\omega_{\mathrm{r}}$ is 0. If the angle between total electromagnetic torque increment and rotor speed oscillation is that $\varphi_{\mathrm{Te}} \in \left[-90^{\circ}, 90^{\circ}\right]$, that is $G_{\mathrm{Tex}} > 0$, which means the variation of total torque increases the amplitude of rotor speed oscillation and the total torque variation negatively damps oscillation, Moreover, the greater the amplitude of G_{Tex}, the greater the negative damping. On the contrary, it acts as a positive damping effect.

Complex torque coefficient method has a clear physical meaning and can get the curve of the electrical damping torque coefficient varying with frequency. However, it is only suitable for the power systems with a fixed frequency AC source, but not for multi-machine systems if there is no fixed frequency source.

6.3.3 Impedance-based modeling and analysis

6.3.3.1 Impedance modeling of components

6.3.3.1.1 Analytical impedance model

The impedance method, originating from the pioneering work of Middlebrook in the 1970s on the input filter design of DC-DC converter [35], has been further extended to general small-signal stability analysis for three-phase AC devices. The external characteristics of these three-phase AC devices are expressed as an impedance model. In other words, if there is a disturbance current ΔI at the terminal of these devices, the voltage response to the disturbance is $\Delta V = Z\Delta I$, and Z is the impedance model.

In recent years, various impedance models have been developed in the synchronous rotating frame (dq-domain) [36] to [38] and stationary frame (abc-phase or sequence-domain) [39] to [41].

All of the state variables in the dq domain remain constant during steady-state operation, to which the linear system theory can then be applied without further complications. Figure 24 presents the dq domain equivalent circuit, where the subscript "0" denotes the steady-state operating point and "Δ" represents its small-signal property. The converter model is composed of two sub-circuits, which are coupled with each other.

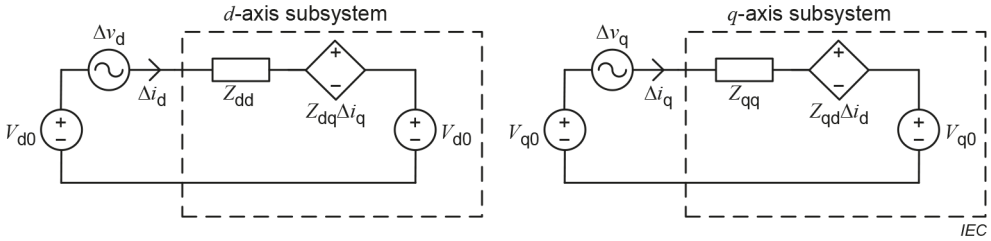

Figure 24 – Three-phase subsystem represented in the dq domain using equivalent small-signal impedance

Neglecting the steady-state components (8) represents the relation of input small-signal voltage and output small-signal current, which is expressed in the Laplace domain. Z_{dq} is defined as the dq impedance.

$$\begin{bmatrix} V_d(s) \\ V_q(s) \end{bmatrix} = \begin{bmatrix} Z_{qq}(s) & Z_{dq}(s) \\ Z_{qd}(s) & Z_{qq}(s) \end{bmatrix} \begin{bmatrix} I_d(s) \\ I_q(s) \end{bmatrix} = \mathbf{Z}_{dq}(s) \begin{bmatrix} I_d(s) \\ I_q(s) \end{bmatrix} \tag{8}$$

Unlike the *dq* domain, state variables in the sequence domain are always time-varying. However, it is found that, under ω_p perturbation in *dq* domain, the dominant frequency components in three-phase variables are $\omega_p + \omega_1$ with the positive sequence and $\omega_p - \omega_1$ with the negative sequence components while other frequencies would be negligible in most of the cases. Thus, the voltage of a three-phase device can be given in (9) by writing one single-phase voltage and identifying the sequence of each component. It is also composed of two sub-circuits, shown in Figure 25, where subscripts 'p' and 'n' represent the positive and negative sequence components of voltage and current, respectively.

$$v_a = V_0 \cos(\omega_1 t + \varphi_{v1}) + \Delta V_p \cos\left[(\omega_p + \omega_1)t + \varphi_{vp}\right] + \Delta V_n \cos\left[(\omega_p - \omega_1)t + \varphi_{vn}\right] \tag{9}$$

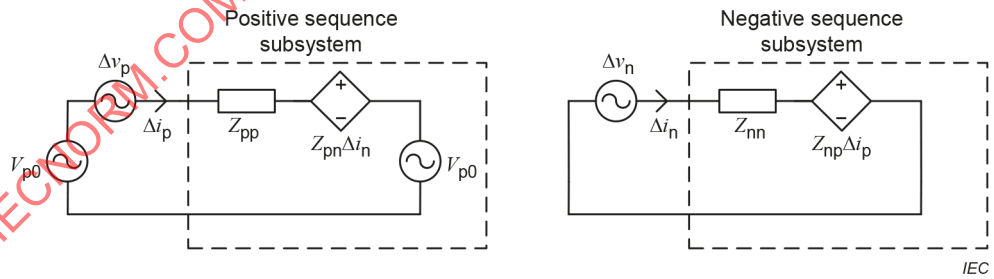

Figure 25 – Three-phase subsystem represented in the sequence domain using equivalent small-signal impedance

With this representation, the small-signal behavior of a three-phase device can be described by an impedance matrix Z_{pn} as given in (10).

$$\begin{bmatrix} V_p(s+j\omega_1) \\ V_n(s-j\omega_1) \end{bmatrix} = \begin{bmatrix} Z_{pp}(s) & Z_{pn}(s) \\ Z_{np}(s) & Z_{nn}(s) \end{bmatrix} \begin{bmatrix} I_p(s+j\omega_1) \\ I_n(s-j\omega_1) \end{bmatrix} = \mathbf{Z}_{pn}(s) \begin{bmatrix} I_p(s+j\omega_1) \\ I_n(s-j\omega_1) \end{bmatrix} \tag{10}$$

The equivalence of the dq impedance and the sequence impedance models has been proved recently, which contributes to the fundamental understanding in the family of the impedance-based stability analysis [42], [43].

The diagonal elements, respectively, represent the positive voltage induced by the positive current and the negative voltage induced by the negative current. Whereas, the off-diagonal elements denote a cross-frequency coupling between the two sequences. Together, the 2 × 2 impedance matrices Z_{pn} represents the impedance model of the system accurately but makes analysis and interpretation complicated.

By different accuracy and computation, sequence impedance can be further divided into original modeling with cross-frequency coupling neglected and modified impedance modeling with all elements considered. It is worth pointing out that the dq impedance is well correlated with the vector control mode commonly used in the existing converter control, which is convenient for the establishment of an analytical model, but not for external testing. Therefore, they generally need to be converted to other domains, such as the positive-negative sequence domain. For the impedance modeling of voltage sourced converter based devices, the consideration of converter control details depends on the required analysis. Based on the control details, the impedance model of a converter can be divided into three categories: 1) considering the inner loop only, 2) considering the inner loop and PLL [44], [45], and 3) considering the outer loop, inner loop and PLL [27], [36], [43].

6.3.3.1.2 Frequency coupling

The frequency coupling effects indicate that if the system is disturbed by a component at a certain frequency, another component at the mirror frequency would also appear. Usually, the original disturbance and its mirror frequencies are expressed as $\omega_p + \omega_1$ with the positive sequence and $\omega_p - \omega_1$ with the negative sequence respectively. With the increase of frequency, the coupling effect will be weakened. It has been proved that the frequency coupling effects can be ignored when analyzing the high-frequency dynamics. However, coupling effects are not negligible in the analysis of medium and low-frequency dynamics such as subsynchronous frequency dynamics [44], [46], [47]. The impedance models, which take the frequency coupling effects into account, are at least 2-dimensional. So a multiple-output (MIMO) model needs to be adopted to incorporate more details to represent the external characteristics of the devices accurately [42], [46].

6.3.3.1.3 Measurement-based impedance model

If the control structures and parameters of a WTG are fully known, its impedance model can be derived using analytical methods. However, for a device with partially or fully unknown configuration or parameters (also called a "black/gray box" device), the impedance model can hardly be obtained using analytical methods.

Taking the impedance model in sequence-frame as an example, the relationship between positive-sequence and negative-sequence components in the presence of coupling is as follows [48].

$$\begin{bmatrix} V_p(s+j\omega_1) \\ V_n(s-j\omega_1) \end{bmatrix} = \begin{bmatrix} Z_{pp}(s) & Z_{pn}(s) \\ Z_{np}(s) & Z_{nn}(s) \end{bmatrix} \begin{bmatrix} I_p(s+j\omega_1) \\ I_n(s-j\omega_1) \end{bmatrix} = \mathbf{Z}_{pn}(s) \begin{bmatrix} I_p(s+j\omega_1) \\ I_n(s-j\omega_1) \end{bmatrix} \tag{11}$$

To characterize the two-by-two impedance matrix, at least two different tests (identified here as test x and test y) are required to solve for the impedance as follows

$$\begin{bmatrix} Z_{\mathrm{p}}(s) & Z_{\mathrm{pn}}(s) \\ Z_{\mathrm{np}}(s) & Z_{\mathrm{n}}(s) \end{bmatrix} = \begin{bmatrix} V_{\mathrm{px}}(s) & V_{\mathrm{py}}(s) \\ V_{\mathrm{nx}}(s) & V_{\mathrm{ny}}(s) \end{bmatrix} \begin{bmatrix} I_{\mathrm{px}}(s) & I_{\mathrm{py}}(s) \\ I_{\mathrm{nx}}(s) & I_{\mathrm{ny}}(s) \end{bmatrix}^{-1} \tag{12}$$

where the subscript px denotes the positive-sequence component of the injection test x, the subscript ny denotes the negative-sequence component of the injection test y, and other subscript combinations follow the same convention.

The impedance matrix (12) can be measured from the simple system in Figure 26.

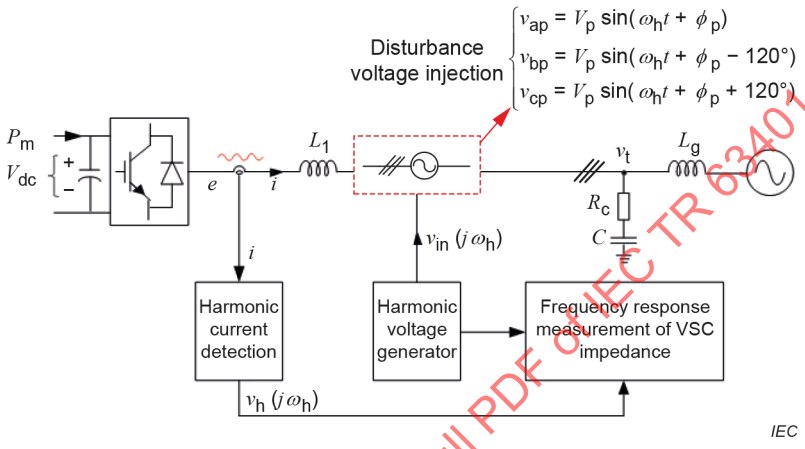

Figure 26 – Impedance measurement in a simple system

First, inject positive sequence voltage with frequency $\omega_p + \omega_1$ into the terminal port of the device and detect the harmonic current with frequency $\omega_p + \omega_1$ and $\omega_p - \omega_1$. Then, inject negative sequence voltage with frequency $\omega_p - \omega_1$ into the terminal port of the device and detect the harmonic current with frequency $\omega_p + \omega_1$ and $\omega_p - \omega_1$. Then the positive-sequence and negative sequence impedances of the device at frequency ω_p can be obtained (12). Repeat the above operations with a wide frequency range, we can obtain the final positive-sequence and negative sequence impedances of the device [49], [50]. A test procedure and specification are recommended in IEC 61400-21-4 (Wind energy generation systems – Part 21-4: Measurement and assessment of electrical characteristics – Test Specifications for Components and Subsystems) for the impedance measurement for power quality studies.

For the dq impedance measurement, we can build the transfer matrix below to associate dq domain variables with sequence domain variables [43].

$$\begin{aligned} \begin{bmatrix} V_{\mathrm{dp}} \\ V_{\mathrm{qp}} \end{bmatrix} &= V_{\mathrm{p}} \begin{bmatrix} 1 \\ -j \end{bmatrix}, \omega_{\mathrm{dq}} = \omega_{\mathrm{p}} - \omega_1 \\ \begin{bmatrix} V_{\mathrm{dn}} \\ V_{\mathrm{qn}} \end{bmatrix} &= V_{\mathrm{n}} \begin{bmatrix} 1 \\ j \end{bmatrix}, \omega_{\mathrm{dq}} = \omega_{\mathrm{n}} + \omega_1 \end{aligned} \tag{13}$$

Therefore, the voltage and current between the dq domain and positive-negative sequence domain can be transformed through the transformations in (14).

$$\begin{bmatrix} V_{\mathrm{d}}(s) \\ V_{\mathrm{q}}(s) \end{bmatrix} = \begin{bmatrix} 1 & 1 \\ -j & j \end{bmatrix} \begin{bmatrix} V_{\mathrm{p}}(s+j\omega_1) \\ V_{\mathrm{n}}(s-j\omega_1) \end{bmatrix}$$
$$\begin{bmatrix} I_{\mathrm{d}}(s) \\ I_{\mathrm{q}}(s) \end{bmatrix} = \begin{bmatrix} 1 & 1 \\ -j & j \end{bmatrix} \begin{bmatrix} I_{\mathrm{p}}(s+j\omega_1) \\ I_{\mathrm{n}}(s-j\omega_1) \end{bmatrix} \quad (14)$$

Since the impedance matrix in dq domain can be presented as

$$\begin{bmatrix} V_{\mathrm{d}}(s) \\ V_{\mathrm{q}}(s) \end{bmatrix} = \begin{bmatrix} Z_{\mathrm{dd}}(s) & Z_{\mathrm{dq}}(s) \\ Z_{\mathrm{qd}}(s) & Z_{\mathrm{qq}}(s) \end{bmatrix} \begin{bmatrix} I_{\mathrm{d}}(s) \\ I_{\mathrm{q}}(s) \end{bmatrix} \quad (15)$$

Then, associating (11), (13) and (15), we can obtain [21]

$$\begin{bmatrix} Z_{\mathrm{dd}}(s) & Z_{\mathrm{dq}}(s) \\ Z_{\mathrm{qd}}(s) & Z_{\mathrm{qq}}(s) \end{bmatrix} = \begin{bmatrix} 1 & 1 \\ -j & j \end{bmatrix} \begin{bmatrix} Z_{\mathrm{pp}}(s) & Z_{\mathrm{pn}}(s) \\ Z_{\mathrm{np}}(s) & Z_{\mathrm{nn}}(s) \end{bmatrix} \begin{bmatrix} 1 & 1 \\ -j & j \end{bmatrix}^{-1} \quad (16)$$

From (16), we can obtain the impedance matrix in the dq domain directly from the sequence-domain impedance matrix.

6.3.3.2 Impedance modeling of a system

The impedance model of a system can be obtained by dividing the system into load and source subsystems, which are characterized by the input and output impedances, respectively. The impedance model can be in the dq domain or sequence domain. Figure 27 shows the system represented by its Thevenin equivalent, where Z_{s} denotes the output impedance of the source side, and Z_{l} indicates the input impedance of the load side. The resultant equivalent circuit of the system can be considered as a control system, in which, Z_{s} and Z_{l} are the functions of 's'. Figure 28 presents the closed-loop with voltage and current as of the input and output of the source and load sides. Therefore, the system open-loop transfer function matrix is

$$\mathrm{H}(s) = Z_{\mathrm{l}}^{-1}(s) Z_{\mathrm{s}}(s) \quad (17)$$

Accordingly, the system closed-loop transfer function matrix is

$$\mathrm{G}(s) = Z_{\mathrm{s}}(s) \left[\mathrm{I} + Z_{\mathrm{l}}^{-1}(s) Z_{\mathrm{s}}(s) \right]^{-1} \quad (18)$$

Usually, the source is stable when unloaded, and the load is stable when powered from an ideal source. The stability of the interconnected system can be solely determined by the system transfer functions, $H(s)$.

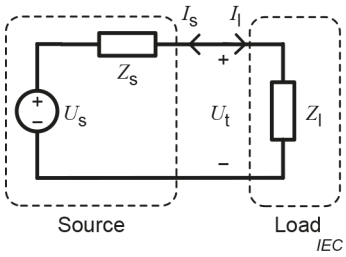

Figure 27 – A simple system in the impedance model, consisting of two separable components: source and load

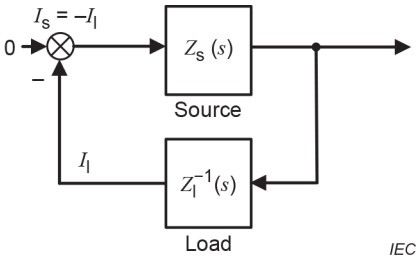

Figure 28 – Impedance model with voltage and current as input and output of the source and load sides; system stability is determined by the two transfer function matrices, $Z_s(s)$ and $Z_l(s)$

However, for a complex large-scale system, it is difficult to divide it into source and load subsystems. To address this problem, the complex system can be modeled as an impedance network, as shown in Figure 29. In the networked impedance model, the original topology is preserved, and each device and line in the system is equivalent to one impedance. Therefore the network contains more details of the original system.

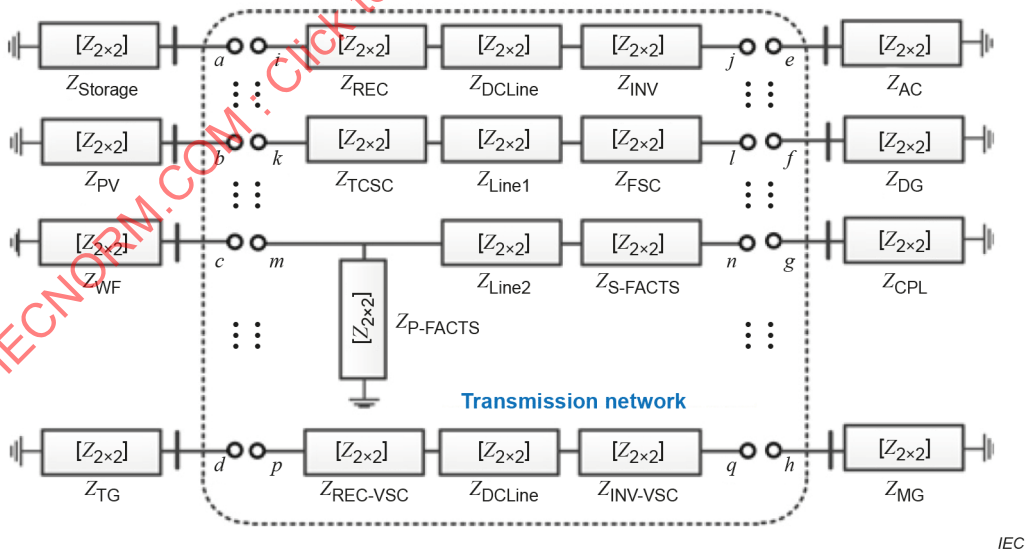

Figure 29 – The unified *dq*-frame INM of a typical power system

It is pertinent to mention that the impedance models in the dq-frame cannot be connected directly due to the different *dq*-frames. The impedance models have to be transferred into a unified *dq*-frame through transformations. In contrast, impedance models in the stationary frame can usually be connected directly without complex transformations.

As a small signal model, the impedance model varies with the operating conditions. Therefore, it is necessary to calculate the power flow before connecting impedance models of components.

6.3.3.3 Impedance model-based analysis

When the whole system is divided into source and load subsystems, the Nyquist criterion can be used to analyze system stability. If the impedances of both source and load subsystems are simplified as a one-dimensional model, the traditional Nyquist criterion can be utilized based on the ratio of source and load impedances. If the two impedances are two-dimensional, the generalized Nyquist criterion (GNC) can be used.

The block diagram in Figure 28 is an equivalent representation of the circuit diagram. Generally, the impedance (*dq* domain or sequence domain) is a 2 × 2 matrix. Thus, the system is a MIMO system, and the stability can be analyzed by the GNC by identifying the minor-loop gain as $H(s)$ [51].

Similarly, the return-ratio matrix, which is calculated from multiplying the source impedance matrix by the inverse of the load impedance matrix (i.e., admittance matrix), can also be applied to analyze the stability.

However, it is very difficult to regard the whole system as two impedances, and $H(s)$ is always a transfer matrix with very high order, which makes it too difficult to utilize the GNC. There has been some research on deriving other stability criteria related to Nyquist. For example, [52] presents several criteria and norms which are more applicable than the Nyquist. Another criterion based on the infinity norm is formulated in [53]. In [54], the stability or damping is jointly judged by the polarity of the real part of the impedance and the slope of the imaginary part at the zero-crossing point where the imaginary impedance vanished. In [55], the Impedance-based stability criterion was extended from the source/load representation into a nodal admittance matrix representation. These papers provided efficient approaches for analyzing larger systems.

6.4 Guidelines on the approaches to SSCI studies

A step-wise procedure is suggested to investigate the SSCI in a practical wind power system. A summary of the procedure is also described in Figure 30. It involves the following steps:

Step 1: The first step is to collect the information about the target system, which includes generation and network topologies, and parameters of the system components, such as WTGs, transmission lines, HVDC lines, nearby STGs, transformers, etc.

Step 2: Next, obtain the upper and lower limits of normal operating conditions, such as wind speed, number of online WTGs, short-circuit ratio, series compensation, etc. If each distinct combination of the values is considered as one operating condition, the total number of operating conditions would be nearly unlimited. In that case, it is almost impossible to model and analyze the system for all operating conditions, because the small-signal impedance model of the WTG has to be re-established for each operating condition. This is one of the issues yet to be addressed. The authors recommend intuitively narrowing down the total number of 'operating conditions' to form a set of critical evaluation conditions by eliminating the safe operating conditions which do not pose the risk of SSCI.

Step 3: For each of the 'critical evaluation condition', construct a representative impedance network model according to the system topology and configuration determined in Step 1. Convert the impedance-network model into lumped impedance to apply the quantitative reactance-frequency crossover approach. If the system is stable, update the set of critical evaluation conditions by excluding the studied combination of operating conditions.

Step 4: In the next step, construct a risk matrix, indicating the most critical to the least severe operating conditions and disturbances constituting the risk of SSCI.

Step 5: Finally, identify the stability or protection boundary and inform the system operator to design and implement a strategy to alleviate the instability risk.

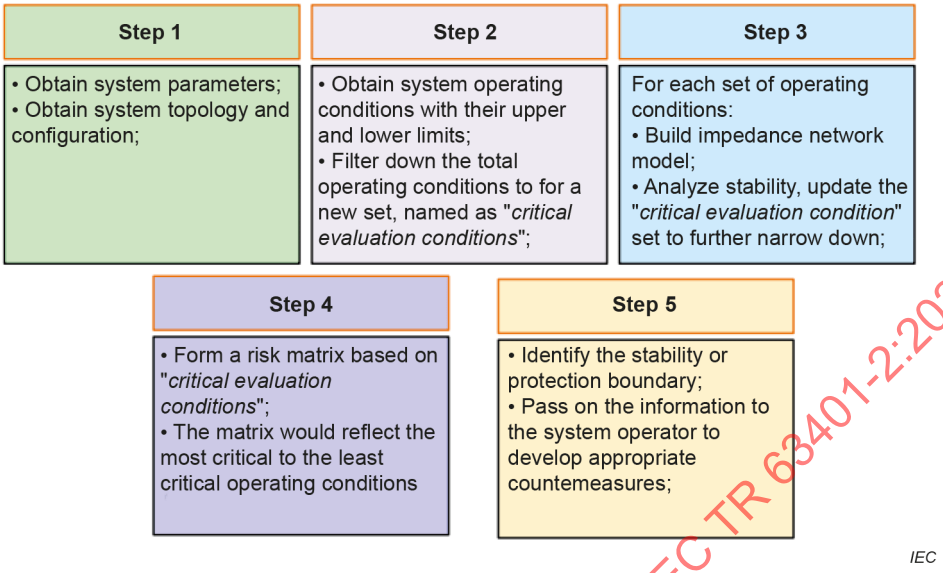

Figure 30 – Recommended guidelines for the SSCI stability analysis of a real-world wind power system

6.5 Clause summary

This clause covered the state-of-the-art conventional and emerging modeling and stability analysis approaches both in time and frequency domains. The modeling requirements and interpretations of analysis results for both time and frequency domain methods are discussed. A comparison is also provided to highlight the strengths and weaknesses of each analysis method in terms of SSCI. Finally, a general procedure and recommended guideline is proposed for carrying out the stability studies for any practical power system.

7 Proposed benchmark models

7.1 Overview

The IEEE SSR working group has proposed the first and second benchmark models to study the classical SSR phenomenon in conventional steam turbines [56], [57]. However, to this date, no benchmark model has been proposed or available for investigating the SSCI in WTGs. In this section, two benchmark system models are proposed, which are based on the Guyuan and Hami wind power systems for studying SSCI in DFIG and FSC-based wind farms, respectively.

7.2 Benchmark model based on Guyuan wind power system

7.2.1 General

This benchmark model is adopted from the Guyuan wind power system located in Hebei Province, China. The actual wind power plant in the Guyuan area contains about twenty-four wind farms. However, a simplified aggregated six-wind farm model is adopted to reproduce the SSCI events and to study the mechanism and characters of the SSCI in DFIG-based systems. The one-line diagram of the six-wind farm system model with series compensated lines is shown in Figure 31. The proposed model incorporates the system details that are sufficient to retain the SSCI phenomenon and its characteristics in DFIG-based wind power systems. It has been used widely used to study many aspects of the SSCI phenomenon. The mechanism and characteristics of the SSCI events have been well investigated in the literature [22], [23].

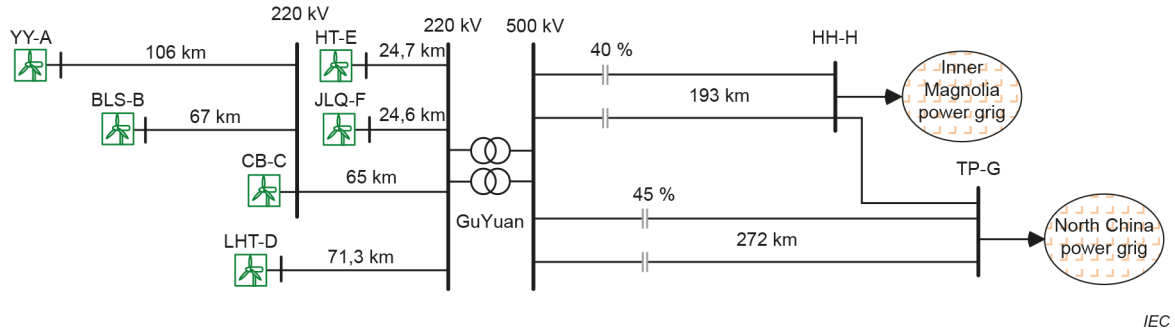

Figure 31 – One-line diagram of the proposed benchmark model adopted from the Guyuan wind power system

7.2.2 Configuration and parameters of the WTGs and Guyuan substation

The six wind farms are situated at different geographical locations, i.e., the distance from each wind farm and Guyuan substation are different, as labeled in Figure 31. The benchmark model consists of six wind farms, namely YY-A, BLS-B, CB-C, LHT-D, HT-E and JLQ-F. The names YY, BLS, CB, LHT, HT, and JLQ represent the abbreviated names of the original substations in the Guyuan wind power system. The wind farms A, B, and C send the generated power to the 220 kV substation. The accumulated power from the 220 kV substation, and the D, E, and F wind farms are then collected at the 220 kV side of the Guyuan substation. For the sake of modeling convenience, the WTGs in all the wind farms are assumed to be of the same make, type, and parameters. These assumptions have a negligible impact on the investigation results. Each wind farm is represented by aggregating the 1,5 MW DFIG according to the total number of DFIGs. The total number of DFIGs in each wind farm is given in Table A.1. The power collected from all the six wind farms is stepped up from 220 kV to 500 kV by a step-up substation transformer. The parameters of the DFIG and the step-up transformers are taken from the real wind power system and are given in Table A.2.

7.2.3 Parameters of the DFIG's converter control

As the name suggests, the SSCI phenomenon is dominantly participated by the DFIG converter controls. The parameters for the rotor side converter (RSC) and grid side converter (GSC) controls of the DFIGs are listed in Table A.3 and Table A.4. The parameters for the inner current controllers of the GSC control are identical. Whereas, the parameters for the inner current controllers of the RSC control are different and are more sensitive to the SSCI characteristics.

7.2.4 Series-compensated electrical network

The six wind farms are radially collected to the Guyuan substation. The generated voltage is stepped up through 0,69/35/500 kV step-up transformers. The generated power is then injected into the main grid of Inner Mongolia and North China via 500 kV double circuit transmissions. The transmission lines are 40 % and 45 % series compensated to enhance their power carrying capacity. The detailed parameters of the series compensated transmission lines are given in Table A.5.

7.2.5 Case study

The proposed benchmark model has been validated through extensive simulation studies [22]. The benchmark model can produce the SSCI events that occurred in the Guyuan wind power system and the associated characteristics can be investigated. Figure 32(a) to (c) shows the simulation results of a typical SSCI event. The current waveform measured at the Guyuan substation and its frequency spectrum shows a 7,4 Hz oscillation. The magnitude and frequency of the SSO component shown in Figure 32(c) are consistent with the actual wind power system. The frequency spectrum was obtained with a window length of 10 s.

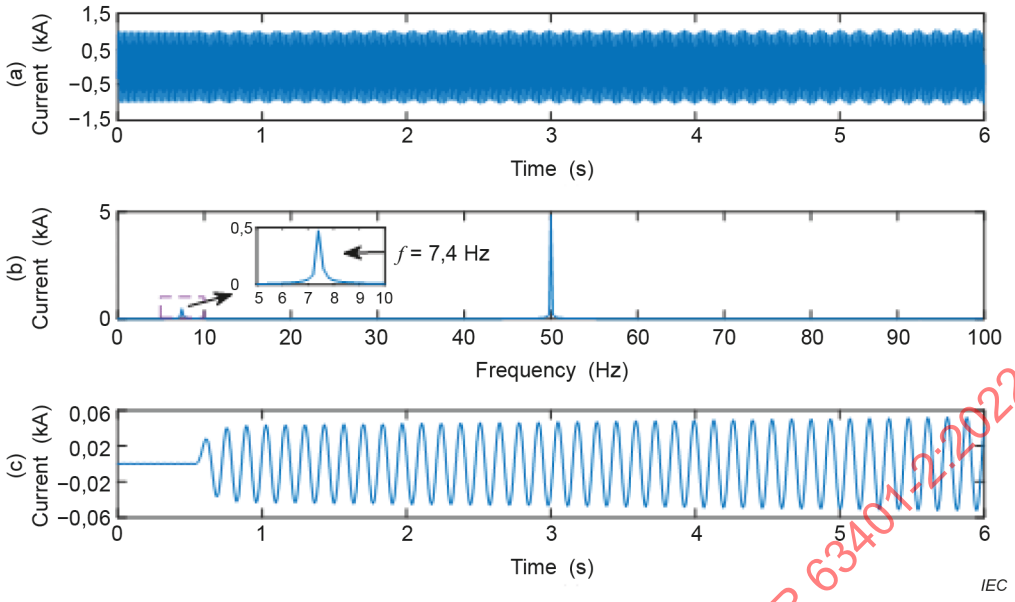

Figure 32 – Simulation results of benchmark model (a) phase A current (b) frequency spectrum of the current (c) subsynchronous current component

7.3 Benchmark model based on Hami wind power system

7.3.1 General

The proposed benchmark model is adopted from the Hami wind power system, which is suitable for studying the SSCI in FSC-based wind farms. The system consists of 733 MVA/660 MW synchronous generators, 1,5 MW FSCs, and ±800 kV line commutated converter (LCC)-HVDC system and 500 kV transmission system, as shown in Figure 33. The electrical, mechanical, and FSC's control parameters are taken from the actual Hami system. Furthermore, the proposed simplified benchmark model is tested to reproduce the actual SSCI event occurred in the Hami wind power system. The modeling is sufficiently detailed to simulate and study various aspects of the SSCI phenomenon in FSC-based wind power systems and nearby turbo-generators.

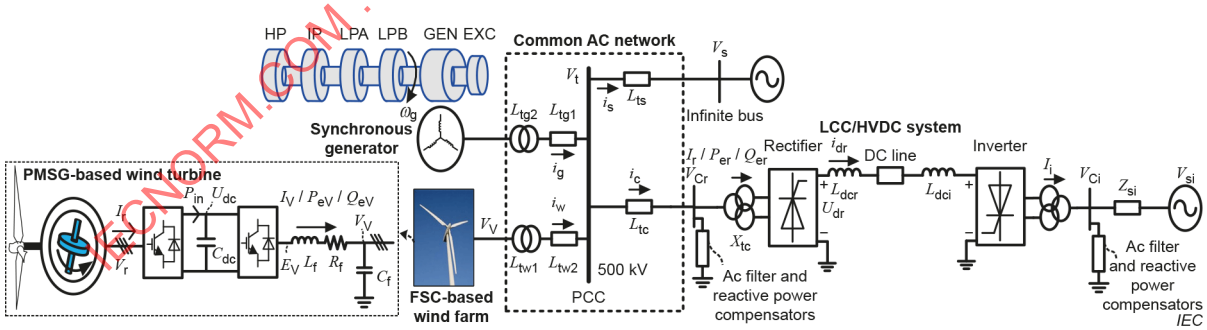

Figure 33 – One-line diagram of the proposed benchmark model adopted from the Hami wind power system

7.3.2 Configuration and parameters of FSCs

FSC is interfaced with the grid through a voltage-sourced converter (VSC). The VSC adopts the decoupled control of active and reactive powers. The inner loops adopt current vector control in the dq reference frame. When the terminal voltage vector is oriented, the d-axis and q-axis currents represent the active and reactive power components, respectively. The outer loop adopts DC voltage control to form active current reference in the d-axis and adopts reactive power control or AC voltage control to form, or directly gives reactive current reference in the q-axis. To realize the terminal voltage orientation, a PLL scheme is adopted. The typical performance requirement for PLL is to be as fast and accurate as possible to detect the phase angle of the terminal voltage.

In the benchmark system, the wind farm contains 300 FSC-based wind turbines, each rated at 1,5 MW, and is represented by an equivalent aggregated model. Table A.6 shows the electrical parameters of the VSC in per unit on the base capacity of the FSC wind turbine.

7.3.3 Configuration and parameters of LCC-HVDC

7.3.3.1 General

The structure diagram of a bipolar LCC-HVDC system is shown in Figure 34, which is different from the first CIGRE HVDC benchmark system [38] used in the case studies in this paper. The rated DC voltage is ±800 kV, the rated power is reduced from 8 000 MW to 800 MW, and the bipolar neutral points are grounded. The model of the LCC-HVDC system includes AC/DC filters, transformers, rectifier/inverter, DC smoothing reactance, and control systems. Each pole of the LCC-HVDC station is composed of two 12-pulse converters in series.

Normally, the rectifier controls the DC line current, while the inverter operates in constant DC voltage or constant extinction angle control. Each converter needs a PLL to realize the terminal voltage orientation.

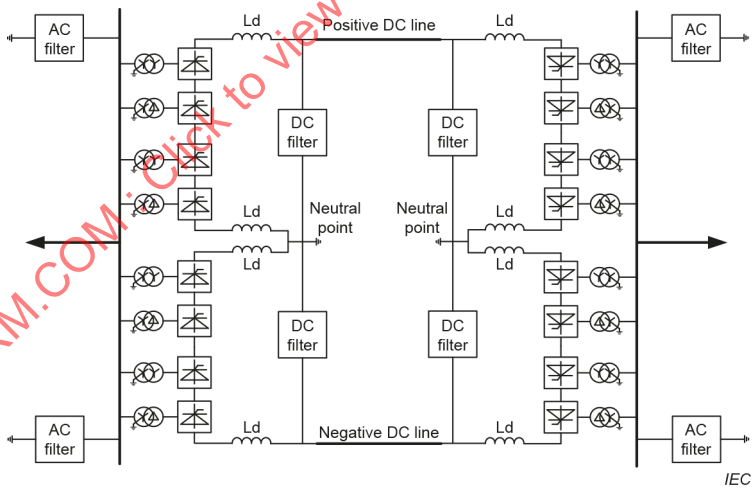

Figure 34 – The structure of the LCC HVDC system

7.3.3.2 DC line and DC smoothing reactance parameters

The length of the DC transmission line is 2 211 km, adopting 6 × JL/G3A-1 000 mm^2 conductors with 6 splits, the resistance of each pole DC transmission line is R_d = 10,65 Ω. The parameter and layout plan of the smoothing reactance is that: the total reactance of each pole is 300 mH, and the layout plan is to divide the smoothing reactance into two parts, which are installed on the pole bus and the neutral bus, respectively, as shown in Figure 34.

7.3.3.3 Parameters of the converter transformer

The LCC-HVC is a ±800 kV DC transmission system. The converter valve is connected in series with 12-pulse valve groups (400 kV+400 kV), and the converter transformer adopts a three-phase double winding transformer. Due to the reduced capacity of LCC-HVDC from 8 000 MW to 800 MW, and the capacity of the converter transformer is reduced correspondingly, but the unit value of the parameter is kept unchanged. The capacity of a single converter transformer is determined according to 1,2 times of the rated active power passed through the converter transformer. The converter impedance is 0,18 pu. There are 8 converter transformers on the rectifier side and the inverter side, respectively. Their parameters at the rectifier side and the inverter side are the same, and the rest of the specific parameters are given in Table A.7.

7.3.3.4 Configuration and Parameters of AC filters

The rated transmission power of DC transmission is 800 MW, and the number of AC filter banks is designed according to the requirements of reactive power. Here, according to 62,5 % of the rated DC power, the reactive powers of rectifier and inverter sides are given as 500MVar.

The AC filters at the rectifier side and the inverter side can be divided into four types: i) double-tuned filter DT11/24 (type A); ii) double-tuned filter DT13/36 (type B); iii) high pass filter HP3; iv) Shunt capacitor. The configuration of the AC filters is shown in Figure 35. See Table A.8 and Table A.9 for specific parameters. If the rated capacity of DC power is increased, the number of AC filter groups needs to be increased accordingly.

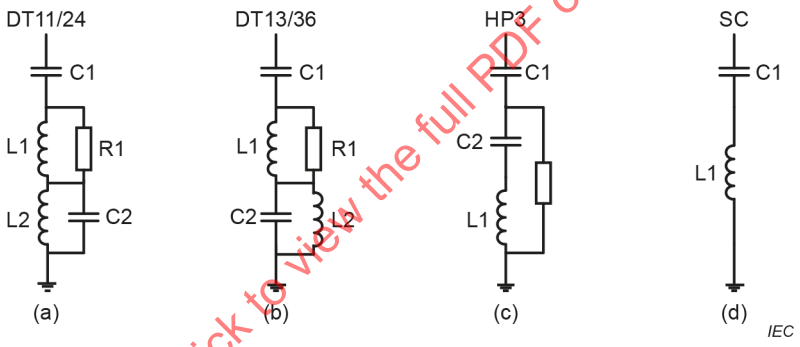

Figure 35 – AC filters and reactive power compensations

7.3.3.5 Configuration and parameters of DC filter

There are two groups of DC filters at the rectifier side and inverter sides, respectively. Each pole is equipped with a group of DC filters, all of which are three tuned passive filtersTT12/24/45. The configuration is shown in Figure 36 and the parameters are given as: C1 = 2,0 uF, L1 = 11,773 mH, C2 = 3,415 uF, L2 = 10,266 mH, C3 = 11,773 uF, L3 = 4,77 mH.

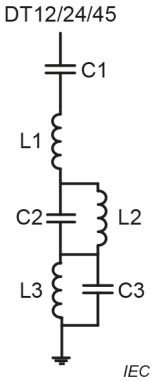

Figure 36 – Three tuned DC filtersTT12/24/45

7.3.3.6 Parameters of Control

Table A.10 shows the control parameters on both the rectifier and inverter sides of the LCC-HVDC system.

7.3.4 Synchronous generators

The synchronous generator model considers the multi-mass spring model of the mechanical system, including high-pressure cylinder HP, low-pressure cylinder LPA, LPB as well as the generator rotor. Since there are low-pass filters in the PSS to filter out the higher frequency components, its influence on the subsynchronous frequency range is small. The dynamic influence of PSS is ignored in the synchronous generator model.

Table A.11 shows the rated parameters and electrical parameters of the synchronous generator per unit on the machine MVA base. Current, voltage and rotor speed are also expressed in per unit.

Table A.12 shows the inertias and spring constants for the spring-mass model. The shafting is a 4-mass model, in which the natural torsional vibration frequencies in the subsynchronous range are 15,86 Hz, 26,64 Hz, and 32,02 Hz. The steady-state mechanical torque is apportioned among the turbine sections HP, LPA, and LPB, respectively as follows: 66 %, 17 % and 17 %.

7.3.5 Electrical network

Figure 37 shows the common electrical network for connecting the synchronous generator, FSC, and LCC-HVDC systems. The infinite voltage bus is a three-phase 50 Hz voltage source with zero impedance at all frequencies. Synchronous generators and VSC-based wind turbine generators are connected to the point of common coupling through set-up transformers and three-phase transmission lines, respectively. Table A.13 shows the common electrical network parameters.

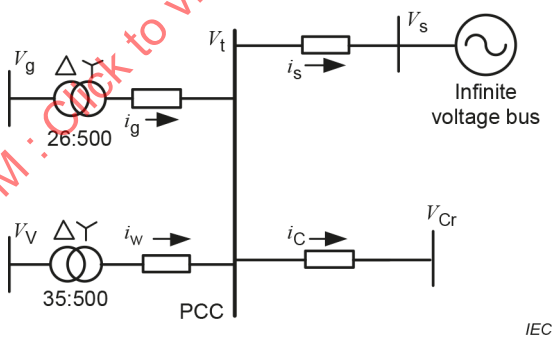

Figure 37 – The common electrical network

7.3.6 Case studies

The proposed benchmark model is validated through simulation studies [22], [58]. Figure 38 shows the simulation results of a typical SSCI phenomenon. The rotor speed wave and its time-frequency analysis clearly show about 16 Hz SSO.

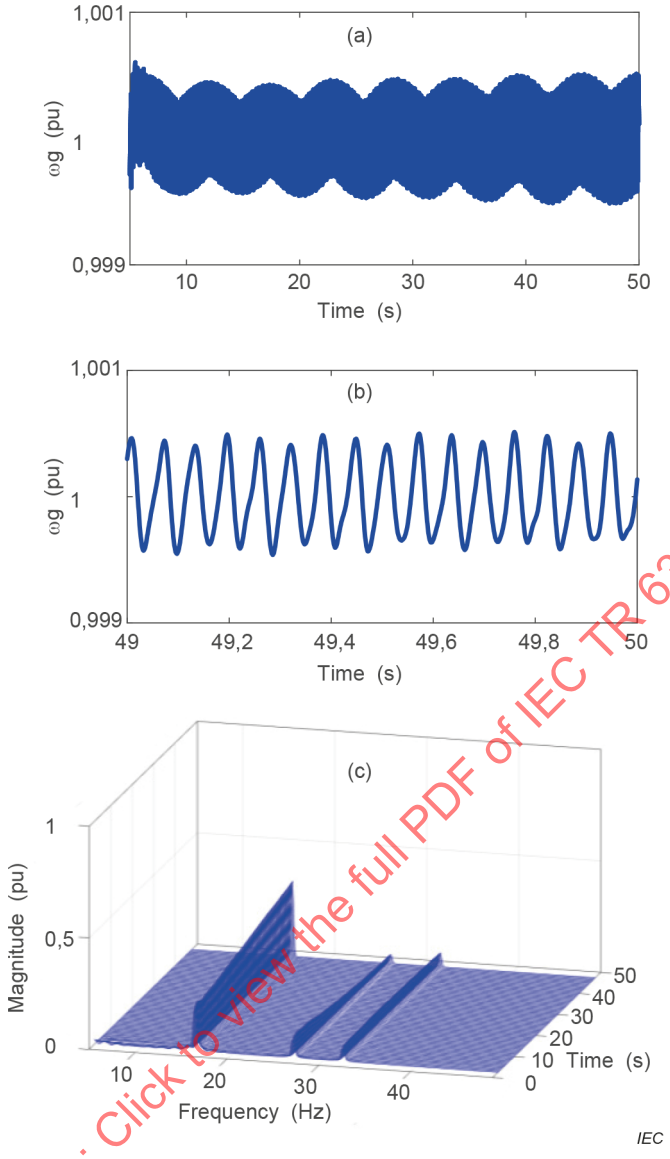

Figure 38 – SSO in the second benchmark model (a) the SG rotor speed (b) subsynchronous frequency component in the speed (c) time-frequency analysis of the rotor speed

7.4 Clause summary

The SSCI in wind power systems is an emerging system stability issue. At present, there are no benchmark models available that could be used to investigate the SSCI. In this clause, two benchmark models are proposed to study the SSCI in DFIGs and FSC wind turbines or PV generators. The proposed benchmark models are simplified and are derived from real-world systems that have experienced SSCI incidents, such as Guyuan and Hami. The benchmark models include the details that are sufficient to retain and reproduce various aspects of the SSCI phenomenon. The electrical, mechanical, and control parameters necessary to reproduce the SSCI incidents are also provided.

8 Mitigation methods

8.1 General

The SSCI is a system-wide phenomenon and thus can be better explained by the system level impedance analysis in the frequency domain. The SSCI occurs when the system's cumulative resistance becomes negative at the subsynchronous frequency. In this context, the potential

remedy to the SSCI problem is to cancel out the negative resistance effect of WTGs or wind farms by reshaping the impedance on either generation or transmission side. Besides other operational measures, a possible mitigation scheme is to add a subsynchronous damping controller (SSDC) at the generator or network sides. The SSDC could then reshape the impedance response at the concerned frequency range, and thus stabilizing the corresponding oscillation modes.

The measures to partially or fully eliminate the risk of SSCI could be taken at various stages of the power system, for instance during the system operation, control, and protection stage [59]. Out of several available mitigation measures, some of the practical schemes are discussed below.

8.2 Bypassing the series capacitor

Under certain operating conditions, the switching of series capacitors in the series compensated transmission lines play can trigger the SSCI. The proper control of the series capacitors installed in the transmission lines can be considered as a temporary solution at the operational schedule. The series capacitors can be bypassed when the unstable oscillation is detected and can be reinserted when there the oscillation is disappeared. Such a capacitor bypass scheme has been proposed and tested in [60].

For example, the Guyuan system experienced several SSCI events when all four series capacitors (referring to system layout shown in Figure 13) are in-service and the total wind power output is less than 10 % of the installed capacity. The field experiences have shown that the SSCI does not occur when one of the four series compensations is brought out of service. This led to a temporary solution, which is temporarily disconnecting one of the four series capacitors of the double-circuit transmission lines when the wind farms' output power is lower than a certain level, e.g., 100 MW in the case of the Guyuan wind power system. This countermeasure of bypassing the series capacitor was adopted by the Guyuan system operator in March 2011. Later on, this output power limit was set to 250 MW instead of 100 MW after the addition of new wind farms in the Guyuan system. The modified countermeasures were adopted by the system operator in April 2014.

A similar method has also been practiced in the ERCOT wind power system. When the SSCI occurs, ERCOT passes the information to system operation to adopt a mitigation measure, for instance, the switching/bypassing the series capacitors as an immediate measure.

8.3 Selective tripping of WTGs

The SSCI occurs when the total system or generation-side resistance is negative a the subsynchronous frequency. On the generation side, the number of in-service WTGs in a wind farm determines the equivalent impedance. During an SSCI event, the degree of participation of a wind farm or WTGs in the interaction is different. Some WTGs participate more and others participate less in the interaction. The unstable SSCI can be stabilized if the number of online WTGs of the most sensitive wind farm are adjusted to reshape the equivalent impedance of the or wind farm. Based on this idea, a system-wide SSCI mitigation scheme can be adopted [61], as shown in Figure 39. The protection scheme consists of several distributed protection relays (DPRs) and a centralized protection coordinator (CPC). The DPRs are deployed at the wind farm substations. Each DPR is responsible for collecting the waveform data of the bus voltage and line currents. It detects and computes the supersynchronous and subsynchronous components and measures the aggregated impedance of each wind farm. The data are time-stamped, packaged, and sent to the CPC through communication links. After receiving the data from all the DPRs, the CPC computes the aggregated impedance model of the whole system. If the aggregated system impedance has a negative resistance at the subsynchronous and/or supersynchronous frequency, the oscillation mode is considered as unstable. The CPC computes the sensitivity-of-tripping index to decide the location and number of wind turbines required to trip for stabilizing the oscillation. The CPC issues the trip commands through communication channels to the DPRs. The data sent to and from CPC include locally measured impedances, frequency of the oscillation mode, and trip commands. The CPC is an additional function or program that can be added to the 'control center'. The identification and tripping

logic functions can be added to existing wide-area measurement systems (WAMs) and centralized control centers [61]. Such a system-wide system utilizes the synch-wave or sub-/super synchronous oscillation enabled WAM/PMUs to monitor and protect the system against the SSCI [62].

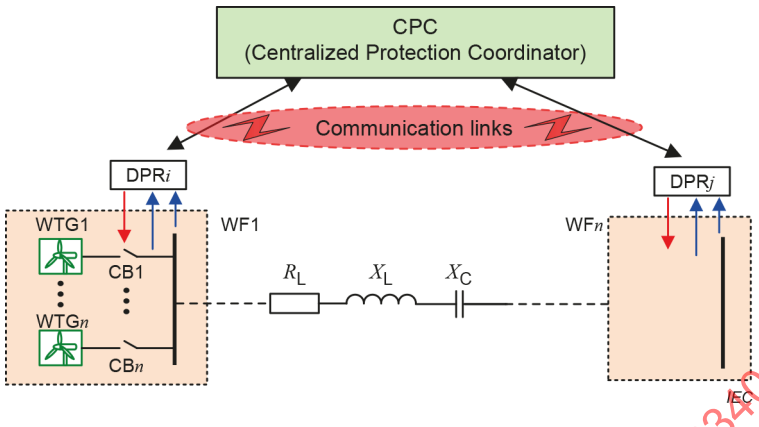

Figure 39 – A system-wide SSCI mitigation scheme based on selective tripping of WTGs

8.4 Network/Grid-side subsynchronous damping controller (GSDC)

The impedance response of the whole wind farm or plant Z_{WF} can be reshaped by adding a special-purpose shunt-connected power electronic converter-based SSDC at the network/grid-side. The grid-side subsynchronous damping controller (GSDC) is a practical scheme, which consists of an SSDC supplemented to a subsynchronous current generator (SCG), as shown in Figure 40(a) and (b) [63]. The basic idea is to modify the impedance characteristics of the system by injecting the currents at the subsynchronous frequency into the system to provide active damping. It consists of two main parts: the SSDC and the SCG. The SSDC utilizes bus voltages and line currents as feedback signals. The subsynchronous currents are extracted and controlled by a combination of properly tuned band-pass and band-stop filters followed by gain and phase shifters. The objective of SCG is to generate an appropriate subsynchronous current that tracks the input reference, or $i_{G\text{-}ref}$, from the SSDC. The SCG is an H-bridge converter with an internal controller.

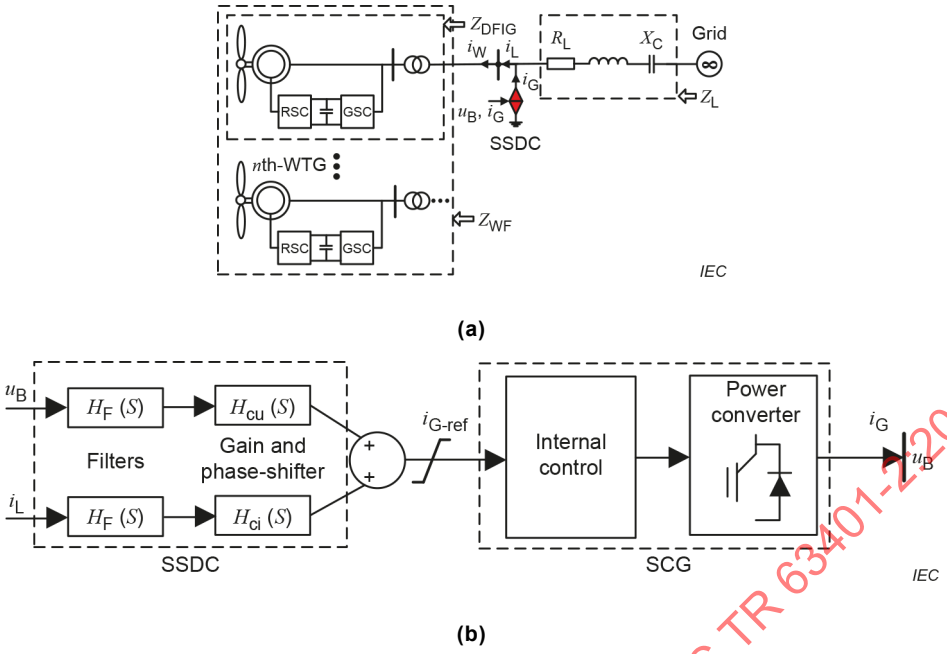

Figure 40 – (a) A series-compensated wind power system with GSDC (b) design and configuration of GSDC including SSDC and SCG

An actual 10 MVA GSDC hardware is developed for the Guyuan system and its damping capability has been validated through CHIL simulations on the Guyuan system's simulation model. The GSDC is connected at the wind farm "C-CB" substation. First, the system is started in steady-state when only 20 % of WTGs are in-service and the wind spend is 6 m/s, generating a total output power of 148 MW. It is an unusual but vulnerable scenario in practice. Then the fourth set of series compensation is switched on that triggered the SSCI. The active power and subsynchronous dynamics of the system are recorded with and without adding GSDC. Figure 40 displays the upstream power of all wind farms, which is measured at the high-voltage side of the transformers. Figure 41 shows the power and subsynchronous currents of the upstream grid with and without GSDC. It can be observed that, without GSDC, the subsynchronous power and current diverge immediately after the switch-on of series compensation, indicating that an unstable SSCI is triggered. After some time, the wind turbine converter controllers reach their limits, resulting in sustained oscillation. When the GSDC is put into service, the oscillation is damped out in a very short time (about 1,5 s) and the system becomes stable.

After validating the damping performance of the GSDC through CHIL tests, it was put into trial operation in 2015. The Guyuan system did not experience the unstable SSCI problem after that.

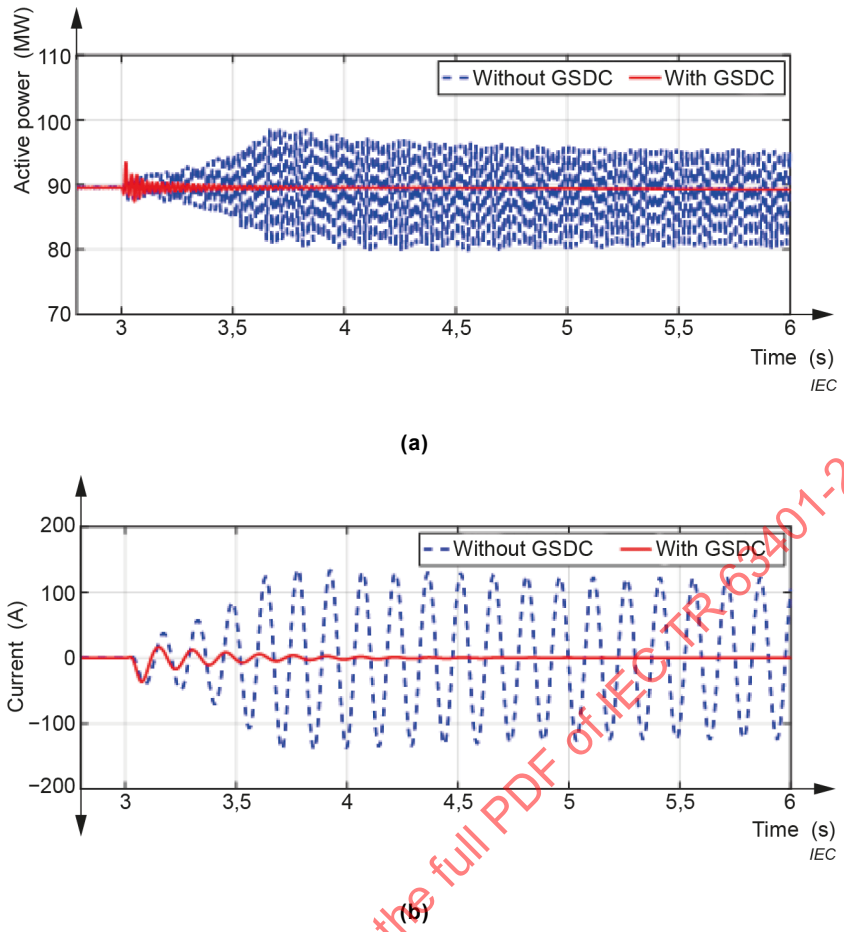

Figure 41 – CHIL test results of GSDC (a) active power (b) subsynchronous current

8.5 Generation-side subsynchronous mitigation schemes

8.5.1 Adjusting the wind turbine converter control parameters

The inappropriate wind turbine converter control settings can enhance the negative resistance effect and thus lead to SSCI. The SSCI can be mitigated by carefully tuning or adjusting the wind turbine converter control parameters. For instance, increasing the coefficient of the proportional controller K_p in the inner current control loop of the GSC can stabilize the SSCI. The CHIL simulation results are presented in Figure 42 when the K_p is multiplied from 1,1 to 1,5. The plots show that the SSCI is significantly attenuated by increasing the K_p. However, the increase of the proportional coefficient may lead to the under-damping of the system in the high-frequency band and induce LC resonance.

Besides adjusting the current loop parameters, the SSCI can also be mitigated by reducing the PLL bandwidth as illustrated in Figure 43. However, it may affect the response of its dynamic process such as power grid fault, and thus it can only be reduced within a certain range.

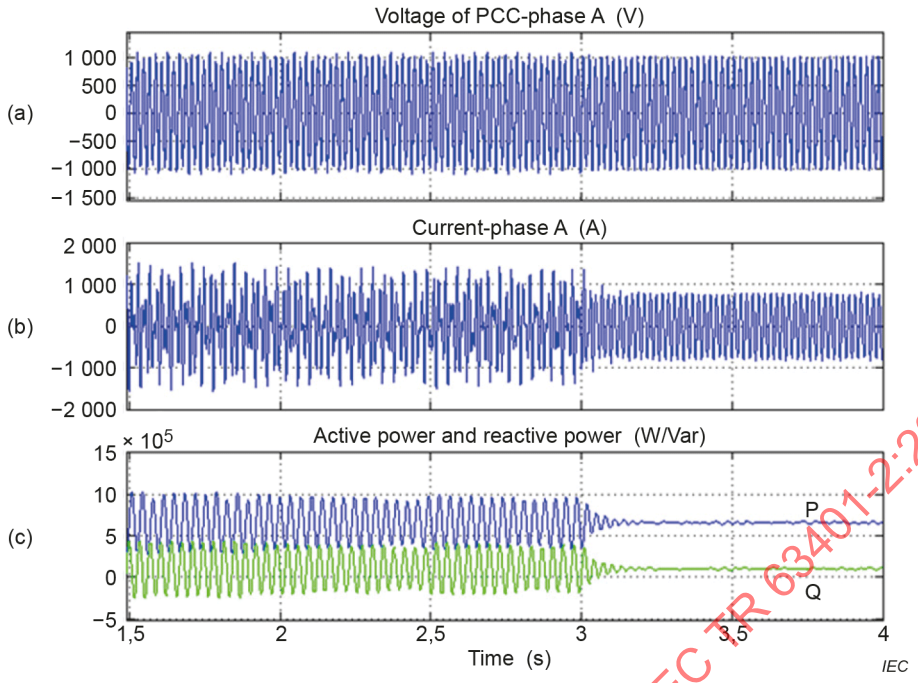

Figure 42 – SSCI mitigation by increasing the K_p of the inner controllers of the GSC (a) voltage at PCC (b) current phase-A (c) active and reactive power

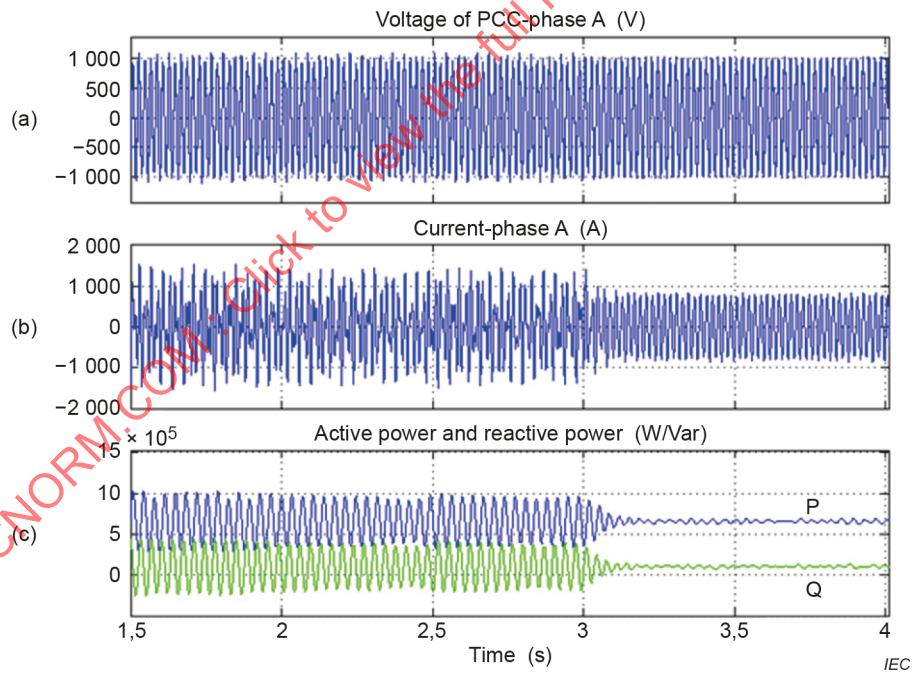

Figure 43 – SSCI mitigation by reducing the PLL bandwidth (a) voltage at PCC (b) current phase-A (c) active and reactive power

8.5.2 Adding an SSDC in the RSC control loop

Similar to the low-frequency oscillation damping in the conventional turbo-generators, the SSO caused by the SSCI can also be suppressed by adding a damping control in the excitation system of each unit with the PSS. By doing so, the damping in the oscillation frequency band of each unit respectively can be increased and the dynamic stability of the entire power grid can be improved. The introduction of a rotor side subsynchronous damping controller can be

understood as a "virtual resistor" which adds positive resistance at the subsynchronous frequency, thus improving the damping at that frequency range.

A typical gain and lead-lag compensator based SSDC added in the d-axis and q-axis loops is depicted in Figure 44. The stator current or the rotor current of the DFIG is used to extract the oscillation component as shown in the schematic block diagram. Next, the lead-lag block is used for phase compensation. Finally, the output is multiplied with gain K, which determines the damping coefficient of the virtual resistance.

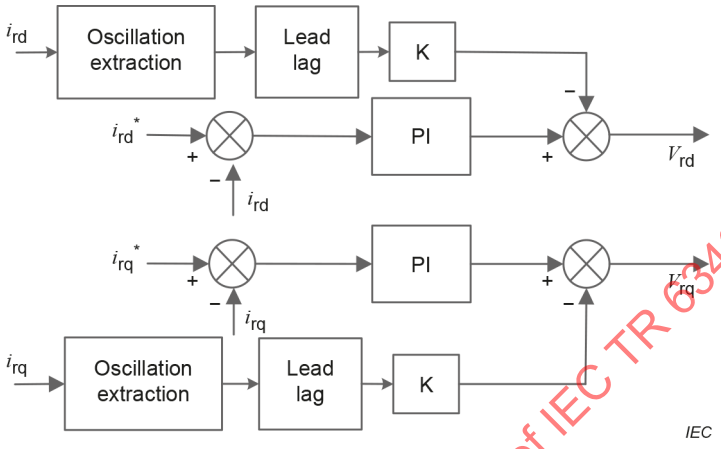

Figure 44 – Control diagram of the virtual resistor for DFIG's RSC controllers

The voltage, current, and active/reactive power plots in Figure 45 show that the SSDC is enabled at 2 s, and the oscillation is attenuated quickly. The damping rate of the subsynchronous frequency current is around 10 % of the original within 250 ms. The active and reactive powers also returned to a steady state. The results show an excellent performance of the SSDC, which adds a virtual resistor in the subsynchronous frequency range.

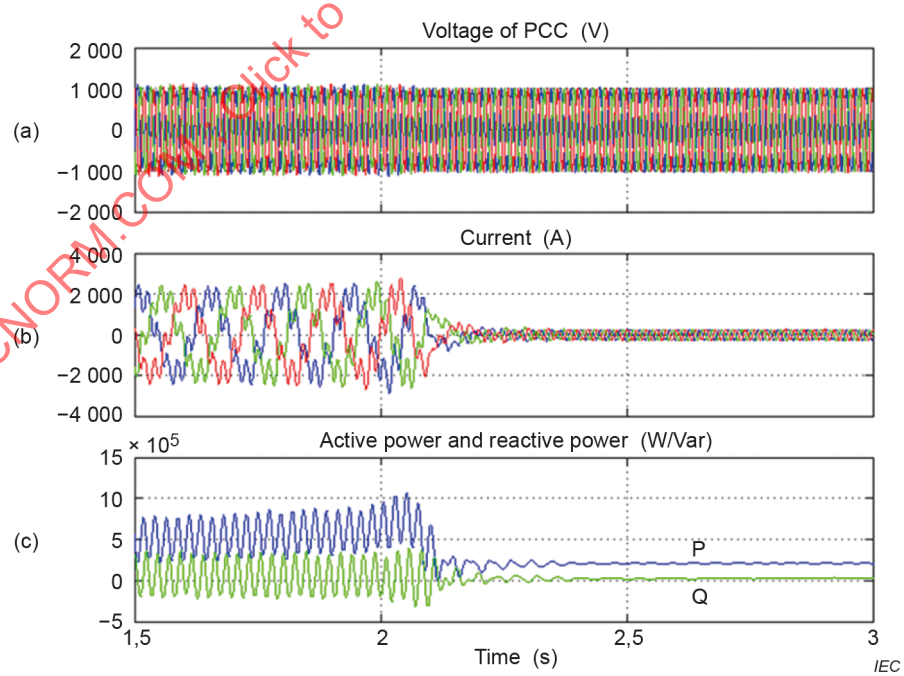

Figure 45 – The SSCI damped out when the virtual resistor is enabled at 2 seconds in simulation (a) voltage at PCC (b) current phase-A (c) active and reactive power

The structure of SSDC can also be based on the gain and proportional derivative controller. In [30], Shair *et al* have validated proportional derivative based SSDC through CHIL and field tests